Metabolic Engineering 95 (2026) 111–130

Contents lists available at ScienceDirect

Metabolic Engineering

journal homepage: www.elsevier.com/locate/meteng

Substrate-informed metabolic engineering of *Corynebacterium glutamicum* enables balanced glucose–xylose co-utilization for the valorization of lignocellulosic feedstocks

David J. Mees, Peng Cao, Ann-Kathrin Thönes, Mario V. Ternes, Michael Kohlstedt, Christoph Wittmann *

Institute of Systems Biotechnology, Saarland University, Saarbrücken, Germany

ARTICLE INFO

Keywords:
Corynebacterium glutamicum
Metabolic engineering
Glucose–xylose co-utilization
^{13}C-tracer analysis
Carbon catabolite repression
Network flux integration
Cardboard hydrolysate
Lysine production

ABSTRACT

Efficient co-utilization of glucose and xylose—the predominant sugars in lignocellulosic and paper-derived hydrolysates—remains a major bottleneck in microbial bioprocessing due to substrate hierarchy and carbon catabolite repression. Here, we develop a substrate-informed metabolic engineering framework in *Corynebacterium glutamicum* that overcomes substrate hierarchy and carbon catabolite repression, enabling a balanced, largely transcription-independent glucose–xylose co-utilization regime at the level of central carbon metabolism. This regime is tailored to the sugar composition of cardboard hydrolysate (CBH), a waste-derived third-generation feedstock. A library of 34 engineered strains was constructed by systematically varying *xylAB* modules, transporter identity, promoter strength, and gene dosage. Integrated physiological, enzymatic, transcriptomic, and ^{13}C-tracer analyses revealed strain XYL-6A as a representative of a distinct, kinetically balanced metabolic regime in which glucose- and xylose-derived fluxes merge early at the F6P/G3P node and maintain stable proportions independent of changing substrate levels or transcriptional adjustments. This regime arises from simple kinetic coordination of a compact, redox-neutral xylose-isomerase pathway with tuned transport capacity, eliminating the need for specialized feeding strategies, extensive regulatory rewiring, or attenuation of native glucose uptake.

The optimized module translated directly into an industrial L-lysine producer, enabling high lysine yields from both defined mixtures and CBH (47.3 mmol C-mol^{-1}). These results demonstrate how substrate-informed pathway design can exploit intrinsic network connectivity to achieve robust mixed-sugar metabolism. More broadly, they illustrate a core synthetic-biology principle: simple, well-balanced modules can generate scalable and reliable metabolic behaviors, providing a practical foundation for valorizing heterogeneous carbon feedstocks.

1. Introduction

Simultaneous utilization of glucose and xylose—the dominant sugars in lignocellulosic and paper-derived hydrolysates—remains a central challenge in microbial metabolism and metabolic engineering (Gárdonyi et al., 2003; Kim et al., 2012). Most microorganisms display strong substrate hierarchies, controlled by carbon catabolite repression (CCR), which prioritizes glucose (Gancedo Juana, 1998; Kaplan Nicholas et al., 2024) while limiting uptake and catabolism of alternative sugars such as xylose (Deutscher et al., 2006). Although this regulatory logic maximizes fitness in natural environments, it restricts metabolic flexibility in industrial bioprocesses where mixed-sugar feedstocks such as lignocellulosic hydrolysates predominate.

Among these feedstocks, paper and cardboard waste represent a particularly relevant resource: despite high recycling rates (Belle et al., 2024), millions of tons of non-recyclable material are still produced annually (Eurostat, 2024). Enzymatic hydrolysis of this residual stream yields cardboard hydrolysate (CBH), which consistently contains glucose and xylose in an approximate 4:1 ratio, corresponding to a xylose:glucose ratio of 0.25 (Kinnarinen et al., 2012a) (Fig. 1). This

* Corresponding author.
E-mail addresses: david.mees@uni-saarland.de (D.J. Mees), caopengsn@gmail.com (P. Cao), ann-kathrin.thoenes@uni-saarland.de (A.-K. Thönes), mario.ternes@uni-saarland.de (M.V. Ternes), michael.kohlstedt@uni-saarland.de (M. Kohlstedt), christoph.wittmann@uni-saarland.de (C. Wittmann).

https://doi.org/10.1016/j.ymben.2026.02.007
Received 16 November 2025; Received in revised form 15 January 2026; Accepted 16 February 2026
Available online 17 February 2026

composition mirrors the composition of hemicellulosic fibers and provides a large, underutilized carbon source for sustainable biomanufacturing (Saha, 2003).

Corynebacterium glutamicum offers a robust and versatile platform for exploiting such substrates. This Gram-positive bacterium combines a well-characterized, modular metabolism with proven industrial relevance in amino-acid and organic-acid production (Ikeda and Nakagawa, 2003; Kalinowski et al., 2003). While *C. glutamicum* does not exhibit classical global CCR systems such as those mediated by CcpA, it lacks a native xylose catabolic pathway, inherently limiting mixed-sugar utilization (Kawaguchi et al., 2006).

Consequently, previous strategies to enable glucose–xylose co-utilization in *C. glutamicum* have included heterologous expression of *xylAB* and related modules, transporter optimization, promoter modulation and gene dosage tuning, as well as adaptive laboratory evolution (Buschke et al., 2013; Ding et al., 2025; Hofer et al., 2025; Werner et al., 2023; Yim et al., 2017). These approaches address different regulatory and kinetic bottlenecks of mixed-sugar metabolism but typically do not explicitly consider flux-ratio stability as a design objective. Consequently, the network-level mechanisms that enable robust and predictable glucose–xylose co-utilization in *C. glutamicum* remain insufficiently understood.

Building on recent advances that have enabled glucose–xylose co-utilization in *C. glutamicum*, including pathway introduction, transporter identification, and adaptive laboratory evolution (Ding et al., 2025), here we sharpen the focus from enabling co-utilization per se to the rational design of a kinetically stabilized co-utilization regime. In many previously reported strains, co-consumption of glucose and xylose can be observed, but the relative uptake rates typically vary with time, substrate composition, or regulatory state, often resulting in shifting or sequential substrate utilization. In contrast, from an engineering perspective, industrial bioprocesses benefit from stable and predictable flux partitioning, particularly when heterogeneous feedstocks with fluctuating sugar compositions are employed.

To address this design challenge, we developed a substrate-informed metabolic-engineering strategy using CBH as a representative industrial feedstock. The approach systematically explores transporter identity, promoter strength, and xylose-pathway balancing to identify self-stabilizing glucose–xylose co-utilization regimes tailored to realistic feedstock compositions. A combinatorial strain library of 34 engineered variants was constructed, systematically varying xylose uptake, phosphorylation, and pathway balance. Integrated physiological, enzymatic, transcriptomic, and ^{13}C-tracer analyses identified strain *C. glutamicum* XYL-6A as a representative of an efficient, largely transcription-independent metabolic regime. In this strain, glucose- and xylose-derived carbons merge early at the fructose-6-phosphate/glyceraldehyde-3-phosphate node, forming a shared central-metabolic pool that maintains constant co-utilization over time, independent of changing substrate levels.

Integration of this balanced co-utilization module into an industrial lysine producer (Becker et al., 2011) demonstrated its translational potential. The resulting strain maintained efficient lysine synthesis from realistic mixed-sugar substrates such as CBH, establishing that finely tuned substrate uptake and pathway balancing can support both metabolic robustness and production performance. Together, these findings illustrate how rational, substrate-informed pathway engineering can leverage intrinsic network connectivity to support stable carbon-flux integration, thereby bridging mechanistic understanding and applied metabolic engineering for efficient utilization of heterogeneous carbon feedstocks.

2. Materials and methods

2.1. Strains, plasmids, and genes

C. glutamicum strains DSM 20300 (ATCC 13032) and LYS-12 were obtained from previous work (Becker et al., 2011). For plasmid amplification, *E. coli* DH10B (Invitrogen, Carlsbad, CA, USA) was used as the host strain. Genomic DNA of *X. campestris* (DSM 3586), *L. brevis* (DSM 20054), and *C. phytofermentans* (DSM 18823) was sourced from the German Collection of Microorganisms and Cell Cultures (DSMZ, Braunschweig, Germany). *E. coli* K-12 MG1655 (Hoffmann et al., 2018)

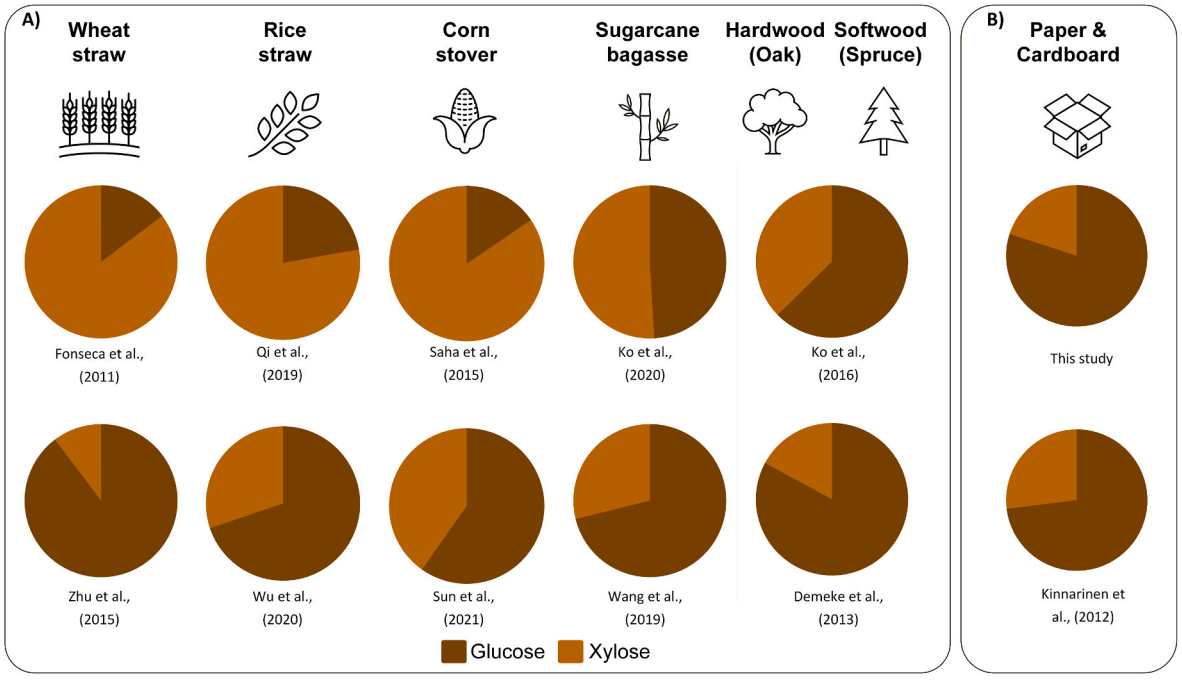

Fig. 1. Glucose and xylose composition of industrially relevant biomass hydrolysates. (A) Reported sugar ratios in hydrolysates derived from wheat straw (Fonseca et al., 2011; Zhu et al., 2015), rice straw (Qi et al., 2019; Wu et al., 2020), corn stover (Saha et al., 2015; Sun et al., 2022), sugarcane bagasse (Ko et al., 2020; Wang et al., 2019), hardwood (Ko et al., 2016), and softwood (Demeke et al., 2013). (B) Characteristic composition of cardboard hydrolysate obtained from non-recyclable paper waste (Kinnarinen et al., 2012a).

and *B. subtilis* 168 (Kohlstedt et al., 2014) were obtained from previous work for genomic DNA extraction. For episomal gene expression in *C. glutamicum*, the plasmid pClik5a MCS was used (Buschke et al., 2011). All *C. glutamicum* strains constructed and analyzed in this study are listed in Table 1, and all plasmids are provided in Table S1 (Supplementary File 1).

2.2. Genetic engineering

Cloning strategies were designed using SnapGene software (version 6.1, GSL Biotech, Chicago, IL, USA) and carried out as previously described (Rohles et al., 2016). DNA fragments were amplified from genomic DNA by PCR using specific primers and the Phusion High-Fidelity PCR Master Mix with HF Buffer (New England Biolabs, Frankfurt am Main, Germany). The plasmid vector was linearized with the restriction enzyme BamHI (FastDigest, Thermo Fisher Scientific, Waltham, MA, USA). Gibson assembly (Gibson et al., 2009) was employed for in vitro assembly of the PCR products with the linearized vector. Constructed plasmids were introduced into *E. coli* DH10B via heat shock transformation (Inoue et al., 1990) and into *C. glutamicum* via electroporation (Becker et al., 2010). Construct integrity was verified by colony PCR using Phire Green Hot Start II PCR Master Mix (Thermo Fisher Scientific) and confirmed by Sanger sequencing (Azenta, Chelmsford, MA, USA). To enable xylose utilization in *C. glutamicum*, various operons were constructed and expressed using the plasmid pClik5α. Operons differed in gene order, gene copy number, and promoter strength, and were placed under the control of either the P_{tuf} promoter (Becker et al., 2005), the P_{sod} promoter (Becker et al., 2007), or a mutated P_{sod} variant, designated $P_{sod,opt}$ (Pauli et al., 2023). Multigene constructs are denoted by concatenated gene symbols (e.g., xylABE, xylAAB, xylABB), indicating operons containing the listed genes in order, each separated by a synthetic ribosome-binding site. For example, xylABE encodes *xylA–xylB–xylE*, whereas xylAAB and xylABB contain duplicated copies of *xylA* or *xylB*, respectively.

Table 1
Strains used in this study.

Strains	Description	Reference
E. coli		
DH10B	Heat shock competent cells for cloning	Invitrogen
C. glutamicum		
ATCC 13032	WT	Becker et al. (2011)
XYL-0	WT + pCLIK5α	This work
Heterologous xylose catabolism		
XYL-1A	WT + pCLIK5α P_{tuf} *xylAB*^{Ecol}	This work
XYL-1B	WT + pCLIK5α P_{tuf} *xylAB*^{Xcam}	This work
XYL-1C	WT + pCLIK5α P_{tuf} *xylAB*^{Lbre}	This work
XYL-1D	WT + pCLIK5α P_{tuf} *xylAB*^{Cphy}	This work
Heterologous xylose transport		
XYL-2A	WT + pCLIK5α P_{tuf} *xylAB*^{Ecol} *xylE*^{Ecol}	This work
XYL-2B	WT + pCLIK5α P_{tuf} *xylAB*^{Xcam} *xylE*^{Ecol}	This work
XYL-2C	WT + pCLIK5α P_{tuf} *xylAB*^{Lbre} *xylE*^{Ecol}	This work
XYL-2D	WT + pCLIK5α P_{tuf} *xylAB*^{Cphy} *xylE*^{Ecol}	This work
Hybrid gene coupling		
XYL-2BC	WT + pCLIK5α P_{tuf} *xylA*^{Xcam} *xylB*^{Lbre} *xylE*^{Ecol}	This work
XYL-2BD	WT + pCLIK5α P_{tuf} *xylA*^{Xcam} *xylB*^{Cphy} *xylE*^{Ecol}	This work
Gene expression balancing		
XYL-3A	WT + pCLIK5α P_{tuf} *xylAAB*^{Ecol} *xylE*^{Ecol}	This work
XYL-3B	WT + pCLIK5α P_{tuf} *xylAAB*^{Xcam} *xylE*^{Ecol}	This work
XYL-3C	WT + pCLIK5α P_{tuf} *xylAAB*^{Lbre} *xylE*^{Ecol}	This work
XYL-3D	WT + pCLIK5α P_{tuf} *xylAAB*^{Cphy} *xylE*^{Ecol}	This work
XYL-4A	WT + pCLIK5α P_{tuf} *xylABB*^{Ecol} *xylE*^{Ecol}	This work
XYL-4B	WT + pCLIK5α P_{tuf} *xylABB*^{Xcam} *xylE*^{Ecol}	This work
XYL-4C	WT + pCLIK5α P_{tuf} *xylABB*^{Lbre} *xylE*^{Ecol}	This work
XYL-4D	WT + pCLIK5α P_{tuf} *xylABB*^{Cphy} *xylE*^{Ecol}	This work
Polycistronic expression strength		
XYL-5A	WT + pCLIK5α $P_{sod,opt}$ *xylAB*^{Ecol} *xylE*^{Ecol}	This work
XYL-5B	WT + pCLIK5α $P_{sod,opt}$ *xylAB*^{Xcam} *xylE*^{Ecol}	This work
XYL-5C	WT + pCLIK5α $P_{sod,opt}$ *xylAB*^{Lbre} *xylE*^{Ecol}	This work
XYL-5D	WT + pCLIK5α $P_{sod,opt}$ *xylAB*^{Cphy} *xylE*^{Ecol}	This work
XYL-6A	WT + pCLIK5α P_{sod} *xylAB*^{Ecol} *xylE*^{Ecol}	This work
XYL-6B	WT + pCLIK5α P_{sod} *xylAB*^{Xcam} *xylE*^{Ecol}	This work
XYL-6C	WT + pCLIK5α P_{sod} *xylAB*^{Lbre} *xylE*^{Ecol}	This work
XYL-6D	WT + pCLIK5α P_{sod} *xylAB*^{Cphy} *xylE*^{Ecol}	This work
Multiplexed optimum genes		
XYL-7A	WT + pCLIK5α P_{sod} *xylAB*^{Ecol} *xylFGH*^{Ecol}	This work
XYL-7B	WT + pCLIK5α P_{sod} *xylAB*^{Xcam} *xylFGH*^{Ecol}	This work
XYL-8A	WT + pCLIK5α P_{sod} *xylAB*^{Ecol} *araE*^{Ecol}	This work
XYL-8B	WT + pCLIK5α P_{sod} *xylAB*^{Xcam} *araE*^{Ecol}	This work
XYL-9A	WT + pCLIK5α P_{sod} *xylAB*^{Ecol} *xylT*^{Lbre}	This work
XYL-9B	WT + pCLIK5α P_{sod} *xylAB*^{Xcam} *xylT*^{Lbre}	This work
XYL-10A	WT + pCLIK5α P_{sod} *xylAB*^{Ecol} *araE*^{Bsub}	This work
XYL-10B	WT + pCLIK5α P_{sod} *xylAB*^{Xcam} *araE*^{Bsub}	This work
Producer strains		
LYS-12	L-lysine overproducer	Becker et al. (2011)
LYS-13	LYS-12 + pCLIK5α P_{sod} *xylAB*^{Ecol} *xylE*^{Ecol}	This work

2.3. Media

The first preculture of *C. glutamicum* was grown in BHI medium (37 g L^{-1} Brain Heart Infusion; Becton Dickinson, Heidelberg, Germany). For the second preculture and main cultures, a defined minimal medium was used. Per liter, the medium contained: 20 g glucose, 5 g xylose, 15 g $(NH_4)_2SO_4$, 1 g NaCl, 200 mg $MgSO_4{\cdot}7H_2O$, 55 mg $CaCl_2$, 20 mg $FeSO_4{\cdot}7H_2O$, 1 mg thiamine HCl, 1 mg calcium pantothenate, 0.5 mg biotin, 100 mL of 2 M potassium phosphate buffer (pH 7.8), 10 mL of a trace element solution (200 mg L^{-1} $FeCl_3{\cdot}6H_2O$, 200 mg L^{-1} $MnSO_4{\cdot}H_2O$, 50 mg L^{-1} $ZnSO_4{\cdot}7H_2O$, 20 mg L^{-1} $CuCl_2{\cdot}2H_2O$, 20 mg L^{-1} $Na_2B_4O_7{\cdot}10H_2O$, and 10 mg L^{-1} $(NH_4)_6Mo_7O_{24}{\cdot}4H_2O$; adjusted to pH 1.0 with HCl), and 30 µg L^{-1} 3,4-dihydroxybenzoic acid. To maintain plasmids, 50 µg mL^{-1} of the appropriate antibiotic was added to the medium. For solid medium, 20 g L^{-1} Difco agar (Becton Dickinson) was added to the liquid formulation. For experiments assessing substrate composition effects, the minimal medium was supplemented with defined glucose–xylose mixtures. Unless otherwise indicated, the standard condition contained 20 g L^{-1} glucose and 5 g L^{-1} xylose (reflecting the 4:1 ratio characteristic of cardboard hydrolysate). Additional mixtures were prepared to vary the glucose:xylose ratio across the full range from 100% glucose (25 g L^{-1}) to 100% xylose (25 g L^{-1}), with intermediate conditions containing 25%, 50%, or 75% xylose at a constant total sugar concentration of 25 g L^{-1}.

Non-recyclable paper and cardboard waste was obtained from Renasci NV (Ostend, Belgium) and subjected to enzymatic hydrolysis, followed by sieving, filtration, and concentration at the Bio Base Europe Pilot Plant (BBEPP, Ghent, Belgium). The concentrated hydrolysate contained glucose (363.7 g L^{-1}) and xylose (83.8 g L^{-1}) in a 4:1 ratio, as well as lactate (19.6 g L^{-1}) and acetate (6.2 g L^{-1}). Prior to use, the hydrolysate was filter-sterilized and diluted to 5% (v/v) in minimal medium to provide sugar concentrations comparable to the defined conditions.

2.4. Cultivation in shake-flasks

Strains were streaked onto BHI agar plates and incubated at 30 °C for 24 h. Single colonies were used to inoculate the first preculture (10 mL BHI in 100 mL baffled shake-flasks), which was grown at 30 °C for 8–16 h in a rotary shaker (230 rpm, 85% humidity; Multitron, Infors AG, Bottmingen, Switzerland). Cells were harvested by centrifugation (3 min, 8800×*g*, room temperature) and used to inoculate the second preculture in minimal medium (25 mL in a 250 mL baffled shake flask). This culture was grown under the same shaking conditions as described above. At mid-exponential growth phase, cells were again harvested (3 min, 8800×*g*, room temperature) and used to inoculate the main culture in minimal medium to an initial OD_{660} of 0.5. Main cultures were grown in biological triplicates (25 mL in 250 mL baffled shake flasks) at 30 °C in a rotary shaker under the same conditions.

2.5. Cultivation in microbioreactors

Medium tests with varying glucose-xylose ratios were performed using a microbioreactor system (BioLector; Beckman Coulter GmbH, Baesweiler, Germany) operated at 1300 rpm, 30 °C, and 85% relative humidity (Kohlstedt et al., 2018). Cultivations were carried out in 48-well microtiter plates with online monitoring of cell growth at 620 nm (OD_{620}) (Becker et al., 2018). Each well was filled with 1 mL of minimal medium containing defined glucose and xylose concentrations. Preculture preparation followed the procedure described above. Main cultures were inoculated to an initial OD_{660} of 0.5.

2.6. Quantification of the cell concentration, substrates, and products

The cell concentration was determined photometrically by measuring the optical density at 660 nm (OD_{660}). The cell dry mass (CDM) concentration was calculated from the measured OD_{660} using a previously determined correlation factor (CDM [g L^{-1}] = 0.32 × OD_{660}) (Rohles et al., 2016). Glucose and xylose were quantified by HPLC using an Agilent 1260 Infinity Series system (Agilent Technologies) (Rohles et al., 2016). Separation was performed on a MetaCarb 87C column (300 × 7.8 mm, 85 °C; Agilent Technologies) with 100% Milli-Q water as the mobile phase at a flow rate of 0.5 mL min^{-1}. Detection was carried out using refractive index detection (1260 RID, G1362A) operated at 55 °C. Concentrations were determined using external standards. Lysine was quantified by HPLC (Agilent 1200 Series) as previously described (Krömer et al., 2005). Samples were diluted 1:10 in a solution containing α-aminobutyric acid (200 μM) as an internal standard. Lysine concentrations were calculated using external standards prepared in the same way (1:10 dilution with 200 μM α-aminobutyric acid).

2.7. Quantification of xylose isomerase and xylulose kinase activities

Cells were harvested during mid-exponential growth phase by centrifugation (5 min, 8800×*g*, 4 °C) and washed with disruption buffer consisting of 100 mM Tris-HCl (pH 7.5), 10 mM $MgCl_2$, and 0.75 mM DTT. The cell pellet was resuspended in the same buffer to a final concentration of 0.25 g cell wet mass mL^{-1}. Aliquots were transferred to lysing matrix B tubes (MP Biomedicals, Eschwege, Germany), and cells were disrupted in a ribolyser (Precellys 24, Bertin Technologies, Ile de France, France) for two cycles of 30 s at 5500×*g*, with a 2-min cooling step on ice between cycles. Cell debris was removed by centrifugation (10 min, 14,000×*g*, 4 °C), and the resulting supernatant was used as crude cell extract.

Xylose isomerase activity was measured using a reaction mixture containing 50 mM Tris-HCl buffer (pH 7.5), 10 mM $MgCl_2$, 0.15 mM NADH, 0.5 U mL^{-1} sorbitol dehydrogenase, and 50 mM D-xylose (Gao et al., 2002; Voronovsky et al., 2005). The mixture was equilibrated at 30 °C for 5 min, and the reaction was initiated by adding 5 μL mL^{-1} of crude extract. The decrease in absorbance at 340 nm, corresponding to NADH oxidation, was monitored over time to determine enzymatic activity. Xylulose kinase activity was determined using a reaction mixture composed of 50 mM Tris-HCl buffer (pH 7.5), 2 mM $MgCl_2$, 0.2 mM NADH, 2 mM ATP, 0.2 mM phosphoenolpyruvate, 10 U mL^{-1} pyruvate kinase, 12.6 U mL^{-1} lactate dehydrogenase, and 8.5 mM D-xylulose (Eliasson et al., 2000). After 5 min of equilibration at 30 °C, the reaction was started by adding 5 μL mL^{-1} of crude extract, and NADH oxidation was measured at 340 nm. Negative controls omitting NADH, D-xylose, D-xylulose, or cell extract were included to verify assay specificity. A molar extinction coefficient of ϵ_{340} = 6.22 L $mmol^{-1}$ cm^{-1} for NADH was used to determine the enzyme activity based on the change in absorbance at 340 nm. Total protein concentrations of the cell extracts were quantified using the BCA assay (Pierce BCA Protein Assay Kit, Thermo Scientific), and enzymatic activities were normalized accordingly.

2.8. Global gene expression analysis

A custom microarray (SurePrint G3 Custom GE 8 × 60K, Agilent Technologies) was designed using the eArray platform (Agilent Technologies) as previously described (Christmann et al., 2023; Pauli et al., 2023). For each gene in the *C. glutamicum* ATCC 13032 genome (KEGG entry: T00102), three distinct 45–60 bp probes were selected. Additional probes were included for the heterologous genes *xylA*, *xylB*, and *xylE* from *E. coli*. Cells were harvested by centrifugation (1 min, 13,000×*g*, room temperature), and the pellets were immediately flash-frozen in liquid nitrogen. Total RNA was extracted using the RNeasy Mini Kit (Qiagen, Hilden, Germany), and RNA concentrations were measured with a NanoDrop 1000 spectrophotometer (PEQLAB Biotechnology, Erlangen, Germany). RNA integrity was assessed using the RNA 6000 Nano Kit on a 2100 Bioanalyzer (Agilent Technologies), and all samples showed RNA integrity numbers (RIN) > 9.0. A total of 50 ng of high-quality RNA was used for labeling. More than 825 ng of Cy3-labeled complementary RNA (cRNA) was synthesized using the RNA Spike-In One-Color Kit and the Low Input Quick Amp WT Labeling Kit (Agilent Technologies), followed by cleanup using the RNeasy Mini Kit (Qiagen). The Cy3 incorporation was confirmed to exceed 15 pmol Cy3 per μg cRNA (NanoDrop 1000, PEQLAB Biotechnology). For hybridization, 600 ng of Cy3-labeled cRNA was applied to the microarray using the Gene Expression Hybridization Kit, hybridization gasket slides, and SureHyb hybridization chambers in a hybridization oven (all from Agilent Technologies). After incubation, slides were disassembled and washed using the Gene Expression Wash Buffer Kit (Agilent Technologies). Microarrays were scanned with the SureScan Microarray Scanner (G4900DA) using the SureScan Microarray Scanner Control Software (v9.1.11.13, Agilent Technologies). Raw data were extracted using the Agilent Feature Extraction Software (v12.1.1.1) and analyzed using GeneSpring software (v14.9, Agilent Technologies). For statistical analysis, a moderated *t*-test was applied, with p-values adjusted for multiple testing using the Benjamini–Hochberg method. A false discovery rate (q-value) cutoff of 0.05 was used, and only genes with a p-value ≤0.05 were considered for downstream analysis (Kohlstedt et al., 2022). RNA extraction, labeling, and microarray hybridization were performed in biological triplicates for each experimental condition. The complete transcriptome dataset has been deposited in the NCBI Gene Expression Omnibus (GEO) under accession number GSE307313.

2.9. GC-MS ^{13}C-tracer studies

For ^{13}C-tracer experiments, *C. glutamicum* cells were cultivated in minimal medium containing 20 g L^{-1} 99% [U-$^{13}C_6$]-glucose and 5 g L^{-1} xylose. Samples were collected during exponential growth at OD_{660} = 4.0 and 8.0. Cells were harvested by centrifugation (5 min, 8800×*g*, 4 °C), the supernatant was discarded, and the pellet was washed twice with deionized water.

For analysis of cellular sugars, 2.5 mg of cell dry mass were hydrolyzed with 250 μL 2 M HCl for 2 h at 100 °C. The hydrolysate was cleared by filtration (Ultrafree-MC, 0.2 μm, Merck Millipore, Darmstadt, Germany), dried under a nitrogen stream, and derivatized by sequential addition of 50 μL methoxylamine (2% in pyridine; 1 h, 80 °C) and 50 μL N,O-bis-trimethylsilyl-trifluoroacetamide (BSTFA; Macherey-Nagel; 30 min, 80 °C). GC–MS analysis was performed as described previously (Kohlstedt and Wittmann, 2019). For proteinogenic amino acid analysis, 1.0 mg of cell dry mass were hydrolyzed with 100 μL 6 M HCl for 24 h at 100 °C. The hydrolysate was filtered (Ultrafree-MC, 0.2 μm), and 50 μL of the filtrate were dried under nitrogen. Subsequently, 50 μL dimethylformamide (0.1% pyridine) and 50 μL N-methyl--N-(tert-butyldimethylsilyl)-trifluoroacetamide (MBDSTFA; Macherey -Nagel) were added for derivatization (45 min, 80 °C) (Wittmann and Heinzle, 2002). GC-MS measurement was performed as described previously (Hoffmann et al., 2018). For fatty acid analysis, cell pellets were dried and transesterified in 300 μL of methanol/toluene/95% H_2SO_4 (50

: 50: 2, v/v/v) for 16 h at 80 °C to convert fatty acids into methyl esters (Dietrich et al., 2023). After incubation, 250 µL of stop solution (0.5 M NH_4HCO_3 + 2 M KCl in H_2O) were added, mixed, and centrifuged (3 min, 8800×*g*, room temperature). The organic phase was analyzed by GC–MS as described previously (Weiland et al., 2025).

All mass-isotopomer distributions (MIDs) were corrected for naturally occurring isotopes (van Winden et al., 2002) and for residual ^{13}C labeling originating from the inoculum. The corrected data thus represent isotopomer fractions of the analyte carbon skeletons. ^{13}C enrichment was expressed as summed fractional labeling (SFL), calculated as described previously (Schwechheimer et al., 2018). SFL values are reported as percentages, where 100% corresponds to complete ^{13}C labeling of the carbon backbone.

3. Results

3.1. Establishing xylose catabolism through heterologous xylAB modules

To systematically establish xylose catabolism in *C. glutamicum*, we constructed synthetic *xylAB* expression modules encoding xylose isomerase (*xylA*) and xylulokinase (*xylB*). Four donor organisms were selected based on reported enzyme activity, cofactor compatibility, and successful heterologous expression in other microbial systems. Modules from *Escherichia coli* K-12 MG1655 and *Xanthomonas campestris*—previously shown to function in *C. glutamicum* (Buschke et al., 2011; Gopinath et al., 2011; Meiswinkel et al., 2013)—served as benchmark references. In addition, *xylAB* from *Clostridium phytofermentans* was included because of the demonstrated activity of its *xylA* gene in

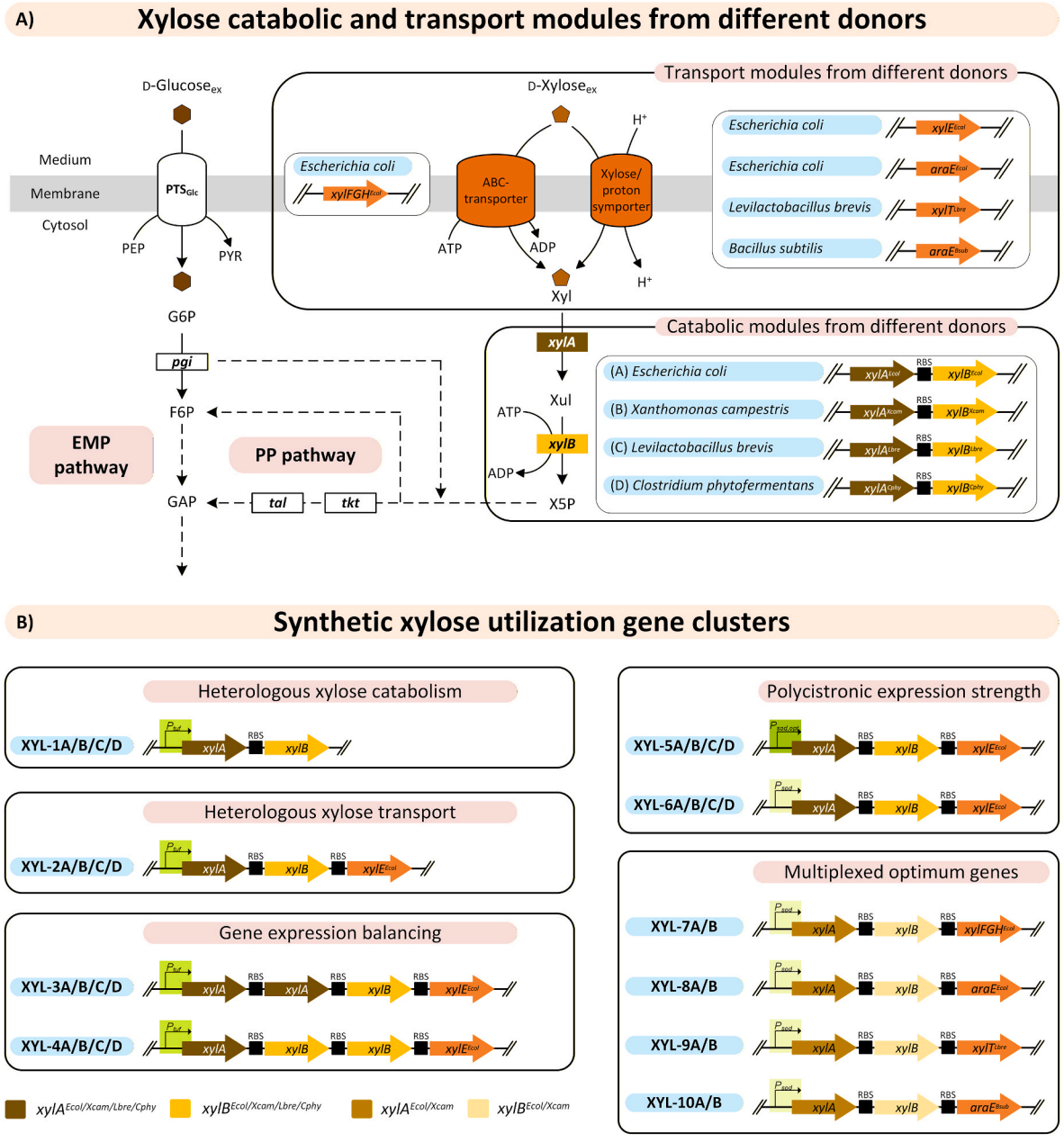

Fig. 2. Substrate-informed metabolic engineering for xylose utilization in *C. glutamicum*. (A) Native glucose uptake/catabolism via PTS_{Glc} and the EMP pathway versus heterologous xylose transport and catabolism via xylose isomerase (XylA) and xylulokinase (XylB). (B) Engineered xylose-utilization modules across ten strain generations differing in donor genes, transporter variants, gene dosage, and promoter strength. Abbreviations: B^{sub}, *B. subtilis*; C^{phy}, *C. phytofermentans*; E^{col}, *E. coli*; F6P, fructose 6-phosphate; G3P, glyceraldehyde-3-phosphate; Glc, glucose; G6P, glucose-6-phosphate; L^{bre}, *L. brevis*; PEP, phosphoenolpyruvate; PP, pentose-phosphate; PYR, pyruvate; EMP, Embden–Meyerhof–Parnas; X5P, xylulose-5-phosphate; X^{cam}, *X. campestris*; Xyl, xylose; Xylu, xylulose.

Saccharomyces cerevisiae (Brat et al., 2009; Demeke et al., 2013), while the *xylAB* operon from *Levilactobacillus brevis* was selected for its natural support of glucose–xylose co-utilization (Kim et al., 2009). All constructs were placed under the constitutive P_{tuf} promoter (Becker et al., 2005), yielding strains XYL-1A to XYL-1D (Table 1, Fig. 2B).

To ensure physiological relevance, strain characterization was performed in a defined medium reflecting the sugar composition of CBH, which contains glucose and xylose at an approximate 4:1 ratio (Kinnarinen et al., 2012a). Accordingly, the test medium comprised 20 g L^{-1} glucose and 5 g L^{-1} xylose (Fig. 3A–D). All recombinants ultimately depleted xylose, confirming pathway functionality, although xylose consumption lagged behind glucose and varied with the donor origin of *xylAB*. Strains harboring the *E. coli* and *X. campestris* modules (XYL-1A and XYL-1B) consumed up to 31 % of xylose before glucose depletion, whereas those expressing the *C. phytofermentans* and *L. brevis* genes (XYL-1C and XYL-1D) reached only 21 % and 18 %, respectively.

These results demonstrate that *xylAB* source selection substantially influences initial xylose utilization kinetics, with the *E. coli* and *X. campestris* modules providing the most effective entry points for *C. glutamicum*. Nevertheless, xylose uptake remained inhibited in the presence of glucose, indicating that carbon catabolite repression was still active and that further engineering of transport or regulatory nodes would be required to enable true co-utilization.

3.2. Enhancing xylose uptake by transporter engineering

Although *C. glutamicum* can import xylose via an endogenous but unidentified transporter (Blombach and Seibold, 2010; Kawaguchi et al., 2006), native uptake capacity is insufficient to support efficient catabolism. To overcome this limitation, a second generation of strains (XYL-2A to XYL-2D) was constructed by introducing the xylose–proton symporter *xylE* from *E. coli* (Yim et al., 2016) (Table 1, Fig. 2B).

Shake-flask cultivations in defined 4:1 glucose–xylose mixtures (Fig. S1, Supplementary File 1) showed that *xylE* expression substantially enhanced xylose assimilation. The co-utilization ratio (CUR; mol xylose mol^{-1} glucose) increased 3.4-fold in XYL-2A and 5.2-fold in XYL-2B compared with their parental strains. In a 4:1 glucose–xylose mixture, the theoretical CUR for proportional consumption is 0.25 mol mol^{-1}. Remarkably, XYL-2A (0.39 mol mol^{-1}) and XYL-2B (0.63 mol mol^{-1}) exceeded this threshold, demonstrating that transporter engineering not only improved uptake capacity but also shifted the metabolic balance toward xylose utilization, even when present as the minor substrate. Consistently, both strains completely depleted xylose before glucose exhaustion (Fig. 3E and F).

In contrast, XYL-2C (0.13 mol mol^{-1}) and XYL-2D (0.28 mol mol^{-1}) remained at or below the expected ratio, indicating that transporter efficiency depends strongly on the *xylAB* module background. Together, these results demonstrate that heterologous expression of *xylE* effectively alleviates transport limitation and partially inverts substrate preference, thereby establishing a crucial step toward balanced glucose–xylose co-utilization in *C. glutamicum* (Kim et al., 2012).

3.3. Efficient glucose–xylose co-utilization requires balanced XylA/XylB activities

To further evaluate the performance of the different xylose catabolic modules, enzymatic activity assays were performed for xylose isomerase (XylA) and xylulokinase (XylB) using cell extracts of the second-generation strains. The control strain XYL-0, carrying the empty plasmid, exhibited only basal XylB activity (0.23 U mg^{-1}), consistent with expression of the native *xylB* gene in *C. glutamicum* (Kawaguchi et al., 2006) (Fig. 4).

Strains XYL-2A and XYL-2B showed markedly elevated and well-balanced XylA/XylB activities (0.80–1.10 U mg^{-1} for both enzymes), whereas XYL-2C and XYL-2D displayed lower XylA activity (0.17–0.38 U mg^{-1}) but high XylB activity (1.30 U mg^{-1}). The more even activity distribution in XYL-2A and XYL-2B correlated with their superior co-utilization ratios (0.39 and 0.63 mol mol^{-1}, respectively), underscoring that coordinated expression of isomerase and kinase functions is essential for efficient xylose metabolism (Xiao et al., 2011).

To test whether xylose flux could be further optimized through enzyme recombination, hybrid modules were generated by combining *xylA* from *X. campestris* with *xylB* from *L. brevis* or *C. phytofermentans*, each coupled with *xylE* from *E. coli*. These constructs yielded strains XYL-2BC and XYL-2BD. Contrary to expectation, neither hybrid enhanced xylose utilization compared with their parental modules. XYL-2BC exhibited a moderate CUR of 0.32 mol mol^{-1} and a reduced specific growth rate (0.23 h^{-1} versus 0.32–0.35 h^{-1} for parental strains XYL-2B and XYL-2C), while XYL-2BD showed minimal co-utilization (CUR = 0.08 mol mol^{-1}) (Fig. S2, Supplementary File 1). These results highlight that efficient glucose–xylose co-utilization requires finely balanced XylA/XylB activity ratios rather than maximal individual enzyme levels. Combining high-activity enzymes from different donors can disrupt kinetic compatibility or cofactor coupling, ultimately constraining flux through the xylose catabolic pathway.

3.4. Gene dosage effects on xylA and xylB expression

To assess the influence of gene dosage on xylose catabolism, additional copies of either *xylA* (XYL-3 generation) or *xylB* (XYL-4 generation) were introduced into the second-generation strains (Table 1, Fig. 2B). The resulting strains were evaluated for growth, sugar utilization, and metabolic performance (Fig. S3, Fig. S4, Supplementary File 1).

Overall, increased gene dosage enhanced xylose consumption in most strains, except for those harboring *xylAB* modules from *L. brevis* (XYL-3D, XYL-4D). The most pronounced improvements were observed in strains derived from *E. coli* modules: XYL-3B (Fig. 3G) and XYL-4A (Fig. 3H) exhibited 4.1-fold and 2.0-fold increases in the CUR, respectively. Notably, XYL-3A achieved the highest CUR of all strains (1.60 mol mol^{-1}) while maintaining a moderate specific growth rate (0.21 h^{-1}) and total carbon uptake rate (22.7 C mmol g^{-1} h^{-1}). This combination—higher xylose utilization with unchanged glucose uptake—indicates a genuine shift in substrate preference rather than a general growth limitation, demonstrating that strong *xylA* expression can actively rewire carbon partitioning between the two substrates. Similarly, XYL-3B and XYL-4B showed moderate CUR increases (1.5- and 1.1-fold, respectively) with no major change in overall growth performance.

Enzyme assays supported these observations. XYL-3B, carrying an additional *xylA* copy, showed a 2.2-fold increase in XylA activity, whereas XYL-4B, with an extra *xylB* copy, exhibited only a 1.5-fold increase (Fig. 4). These nonlinear responses confirm that gene amplification does not translate directly into proportional enzyme activity (Sasaki et al., 2008). The attenuated XylB increase in XYL-4B may reflect post-transcriptional or translational constraints limiting enzyme synthesis or stability. Together, these results demonstrate that elevating *xylA* or *xylB* expression enhances xylose assimilation in a context-dependent manner. Maintaining balanced enzyme activities is crucial for efficient co-utilization, whereas disproportionate *xylA* overexpression can induce a distinct xylose-first metabolic state—a phenotype explored in more detail below.

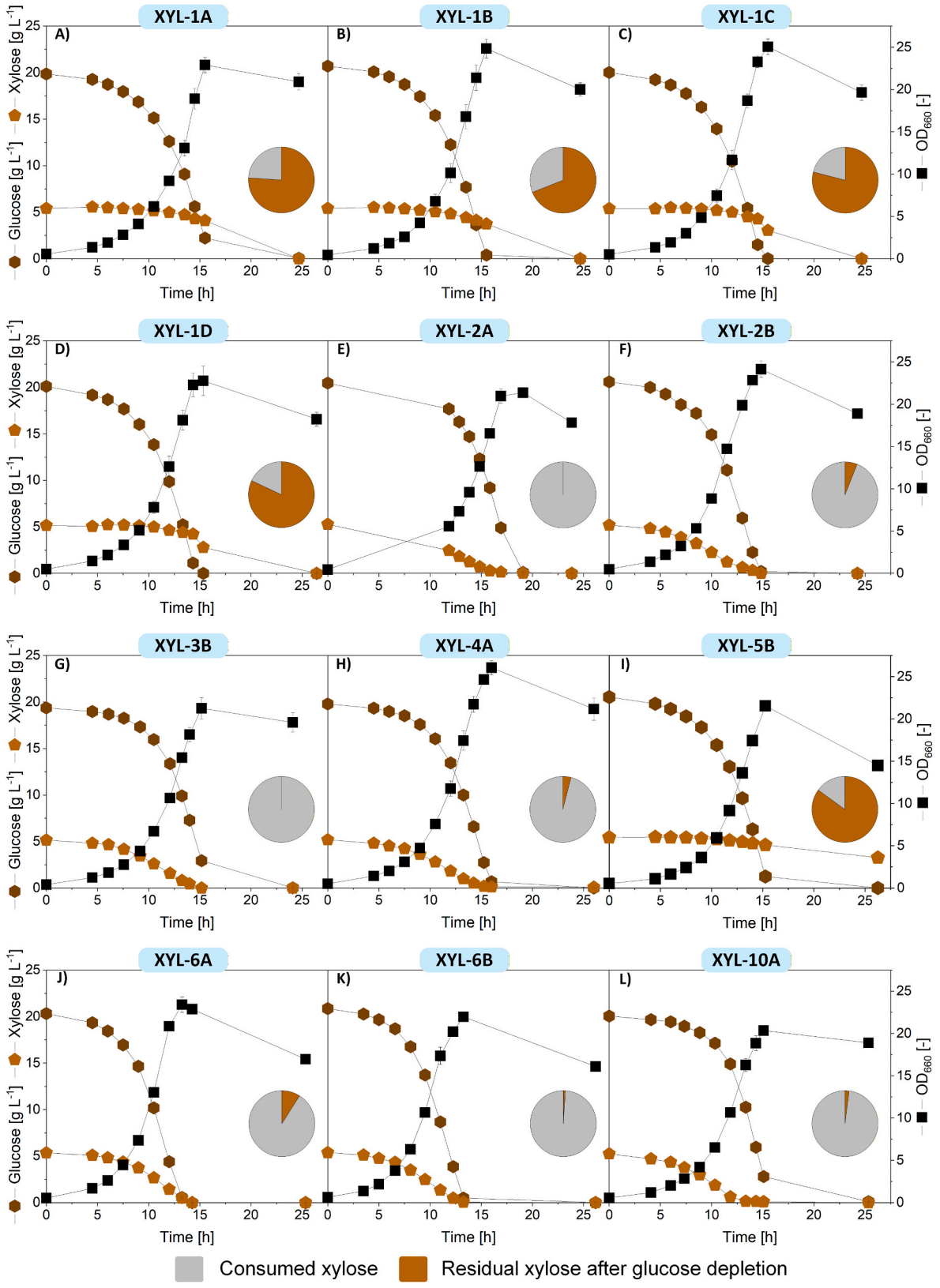

Fig. 3. Cultivation profiles of *C. glutamicum* strains carrying different xylose catabolic modules. Strains were cultivated in minimal medium with 20 g L^{-1} glucose and 5 g L^{-1} xylose. Circular insets show residual (brown) and consumed xylose (grey) at the time of glucose depletion. Data are means ± s.d. (biological triplicates). (For interpretation of the references to colour in this figure legend, the reader is referred to the Web version of this article.)

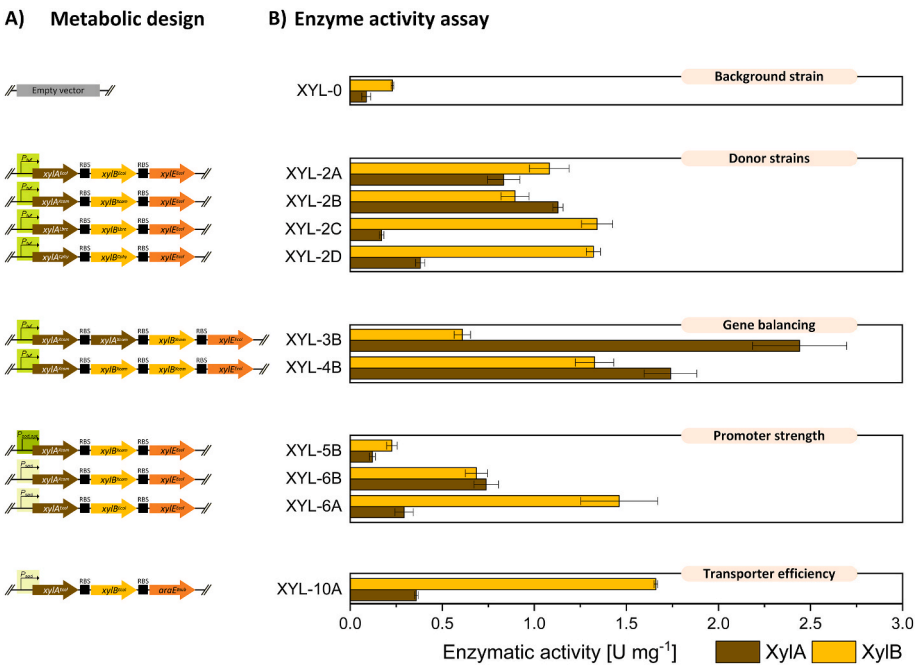

Fig. 4. XylA and XylB activities in engineered *C. glutamicum* strains. (A) Background activity in control strain XYL-0, unable to utilize xylose (Fig. S13, Supplementary File 1) (B) Donor-module comparison in second-generation strains. (C) Gene-dosage effects in strains with additional *xylA* or *xylB* copies. (D) Promoter-strength effects in fifth- and sixth-generation strains. (E) Activities in the transporter-engineered tenth-generation strain XYL-10A. Activities are in U mg^{-1} protein. Data are means ± s.d. (biological triplicates).

3.5. Promoter strength determines efficiency of polycistronic *xylAB* expression

To assess how transcriptional strength affects coordinated *xylAB* expression, two further generations of strains were constructed. The fifth-generation variants expressed the xylose pathway under the strong synthetic promoter $P_{sod,opt}$ (Pauli et al., 2023), while the sixth generation employed the weaker native P_{sod} promoter (Becker et al., 2007) (Table 1, Fig. 2B). All constructs also carried the *xylE* transporter to ensure sufficient substrate uptake (Fig. S5, Fig. S6, Supplementary File 1).

The results revealed a striking inverse correlation between promoter strength and performance. Strains harboring $P_{sod,opt}$ displayed poor xylose utilization: XYL-5B (Fig. 3I) and XYL-5D showed almost no xylose consumption, whereas XYL-5A and XYL-5C initiated xylose metabolism only after glucose depletion, exhibiting diauxic rather than co-utilization behavior(Fig. S5, Supplementary File 1). Despite higher transcription, effective XylA/XylB activities were markedly reduced, consistent with translational burden or misfolding at excessive expression levels. In contrast, strains expressing *xylAB* under the weaker P_{sod} promoter—XYL-6A and XYL-6B—initiated xylose uptake before glucose exhaustion and completed full co-utilization within 13.5 h (Fig. 3J and K). Both strains reached co-utilization ratios of 0.35–0.49 mol mol^{-1} and achieved among the highest observed in the strain library. Although XYL-2D grew slightly faster (0.37 h^{-1}), it primarily consumed glucose, whereas XYL-6A and XYL-6B maintained balanced uptake of both sugars.

To clarify the mechanistic basis of this difference, XylA and XylB activities were quantified for XYL-5B and XYL-6B. Despite stronger transcription, XYL-5B retained only 10 % of XylA and 25 % of XylB activity relative to the second-generation strain (Fig. 4). In contrast, XYL-6B retained 65 % and 76 % activity under the weaker promoter. These results demonstrate that excessive transcriptional strength impairs effective enzyme formation, likely through translational burden, improper folding, or metabolic feedback. Direct quantification of transcript levels was not feasible because plasmid-encoded *xylA* and *xylB* sequences generate strong background in qPCR assays, obscuring promoter-specific differences. Nevertheless, the marked decrease in enzyme activity despite stronger promoters implies that the loss of function occurred post-transcriptionally rather than from promoter malfunction, consistent with translational burden or misfolding at excessive expression levels. Taken together, the data reveal that moderate promoter strength ensures functional expression and pathway balance, whereas overexpression destabilizes the system. The P_{sod}-driven strains XYL-6A and XYL-6B therefore represent optimized co-utilizers, combining efficient xylose uptake with balanced flux through the heterologous pathway and defining the most favorable expression regime identified in this study.

3.6. Fine-tuning co-utilization via alternative transporter selection

Strains XYL-6A and XYL-6B, which exhibited balanced glucose–xylose co-utilization, served as the chassis for further optimization through the evaluation of alternative xylose transport systems. Four transporter candidates from diverse donor organisms were tested to examine how uptake mechanism influences substrate hierarchy: the ABC-type transporter *xylFGH* and the arabinose–proton symporter *araE* from *E. coli*; the xylose–proton symporter *xylT* from *L. brevis*; and the *B. subtilis araE* symporter (Table 1, Fig. 2B). Each transporter gene was expressed under the P_{sod} promoter in the sixth-generation background, yielding strains XYL-7 ($xylFGH^{Ecol}$), XYL-8 ($araE^{Ecol}$), XYL-9 ($xylT^{Lbre}$), and XYL-10 ($araE^{Bsub}$) (Fig. S7–S10, Supplementary File 1).

Among these, only expression of *araE* from *B. subtilis* (in strains XYL-10A and XYL-10B) significantly altered substrate utilization behavior. These variants deviated from the canonical glucose-first hierarchy of *C. glutamicum*, exhibiting a pronounced shift toward xylose uptake. Co-utilization ratios reached 1.38 mol mol^{-1} (XYL-10A; Figs. 3L) and 1.09 mol mol^{-1} (XYL-10B), indicating that xylose uptake exceeded glucose uptake even though glucose remained the dominant substrate in the parental strains. This redistribution of substrate flux was accompanied by a moderate reduction in growth rate (0.29 h^{-1} and 0.26 h^{-1}, respectively) but did not impair overall performance.

These findings demonstrate that transporter identity exerts a decisive influence on carbon flux partitioning. In particular, the *B. subtilis araE* symporter establishes a xylose-preferential metabolic regime in *C. glutamicum*, effectively inverting the canonical substrate hierarchy while sustaining robust growth. This outcome underscores that targeted modulation of transport functions can serve as a powerful strategy to reshape carbon utilization patterns in mixed-sugar bioprocesses. It should be noted that the observed differences between transporter variants reflect their functional performance *in vivo*, integrating intrinsic transport properties with expression level, membrane context, and energetic coupling, rather than isolated kinetic parameters determined in vitro.

3.7. Benchmarking engineered C. glutamicum strains and validation on cardboard hydrolysate

A total of 34 engineered *C. glutamicum* strains were constructed and characterized, spanning the full range of xylose-utilization phenotypes—from no uptake in XYL-0 to variants preferentially consuming xylose over glucose (Fig. 5), with differences in growth (Fig. S11, Supplementary File 1). To identify optimal candidates for cardboard hydrolysate (CBH) valorization, benchmarking was performed using the native sugar composition of the feedstock as the design reference. CBH typically contains glucose and xylose in an approximate 4:1 glucose: xylose ratio, corresponding to a xylose:glucose ratio of 0.25 (Kinnarinen et al., 2012). Accordingly, three quantitative criteria were defined to capture both metabolic balance and industrial relevance: (i) a specific growth rate ($\geq$0.30 h^{-1}) as a proxy for overall fitness and productivity; (ii) a CUR (xylose:glucose $\geq$0.3 mol mol^{-1}), ensuring that xylose consumption proceeds proportionally to—or slightly above—the 0.25 ratio characteristic of CBH; and (iii) a specific substrate uptake rate ($\geq$30 C mmol g^{-1} h^{-1}) as a measure of metabolic throughput and predictor of volumetric productivity.

Only a subset of strains fulfilled all three benchmarks. Four variants exceeded both the growth-rate and CUR thresholds (Fig. 6A), while ten met the growth and uptake-rate criteria (Fig. 6B). Notably, three strains—XYL-2B, XYL-6A, and XYL-6B—satisfied all benchmarks simultaneously. These variants effectively exploited the mixed-sugar composition of CBH, achieving robust growth while consuming xylose and glucose in parallel at balanced rates. Strikingly, XYL-6A and XYL-6B maintained a fixed proportional uptake ratio of glucose and xylose throughout the entire cultivation, leading to the near-simultaneous depletion of both substrates, independent of their availability (Fig. 6C).

To validate these results under process-relevant conditions, the top-performing strains were cultivated on CBH as the sole carbon source (Fig. 7). The hydrolysate, derived from non-recyclable paper waste, contained primarily glucose (363.7 g L^{-1}) and xylose (83.8 g L^{-1}) at a ratio of approximately 4:1, as well as lactate (19.6 g L^{-1}) and acetate (6.2 g L^{-1}). After dilution to cultivation concentrations, all strains displayed strong growth. Xylose was depleted concurrently or slightly before glucose, confirming that the co-utilization phenotypes observed in defined media were fully retained on the complex substrate. Growth dynamics on CBH closely mirrored those on synthetic sugar mixtures: XYL-6A and XYL-6B maintained high specific growth and co-utilization rates, whereas XYL-2B exhibited slightly lower substrate uptake yet remained metabolically robust.

The presence of lactate and acetate did not impair growth, reflecting the high tolerance and metabolic versatility of *C. glutamicum*. Both organic acids were co-consumed with the sugars during early exponential growth and completely depleted within 5 h. At high cell density (OD_{660} about 30), a transient re-accumulation of lactate occurred but was rapidly re-assimilated after sugar depletion, likely reflecting a short-

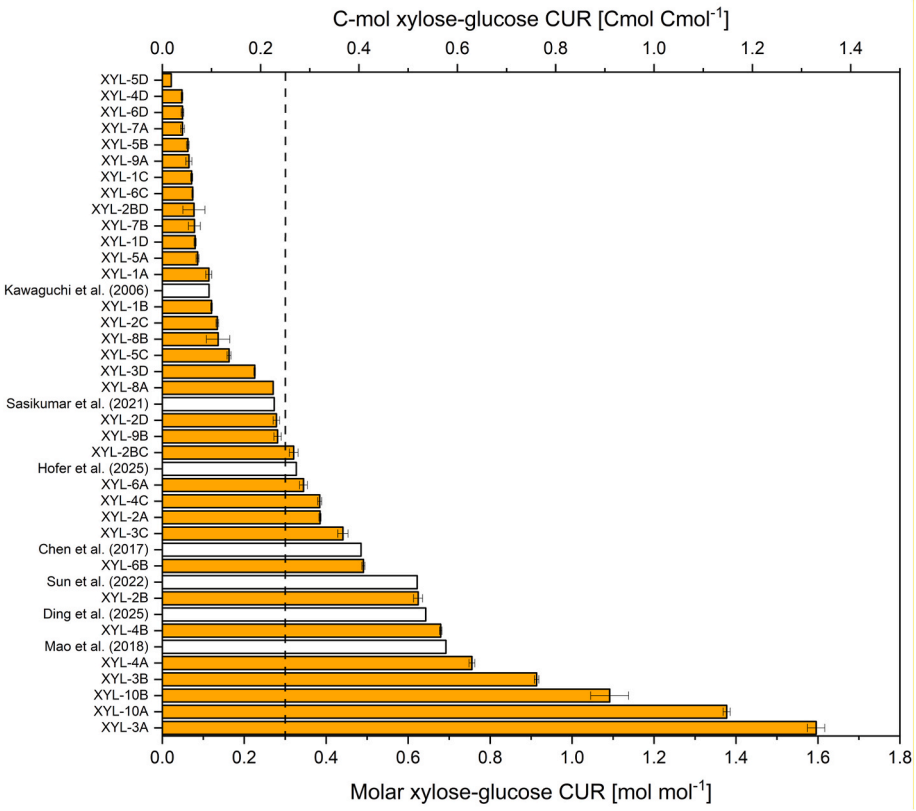

Fig. 5. Xylose:glucose co-utilization ratios (CURs) of engineered *C. glutamicum* strains. Ratios are given as mol xylose·mol^{-1} glucose. For carbon-normalized plots, C-mol C-mol^{-1} was additionally used where indicated. The dotted line marks the 0.30 mol mol^{-1} threshold to ensure xylose depletion at the 1:4 CBH ratio. Literature benchmarks are included for comparison (Kawaguchi et al., 2006; Sasikumar et al., 2021; Chen et al., 2017; Hofer et al., 2025; Sun et al., 2022; Ding et al., 2025; Mao et al., 2018). Data are means ± s.d. (biological triplicates). (For carbon-normalized plots, C-mol·C-mol^{-1} was additionally used where indicated.)

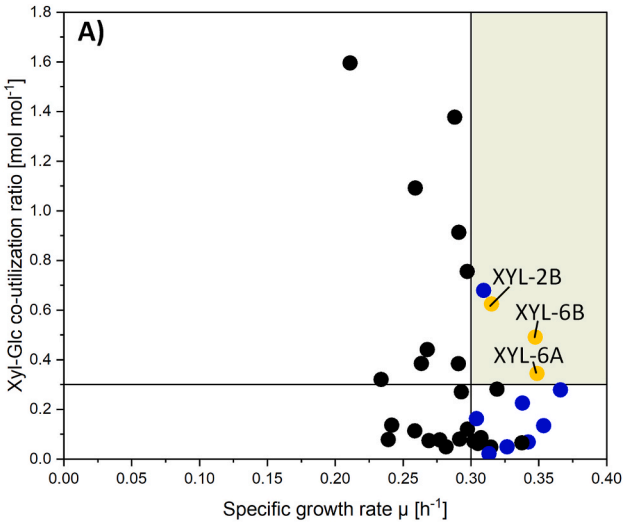

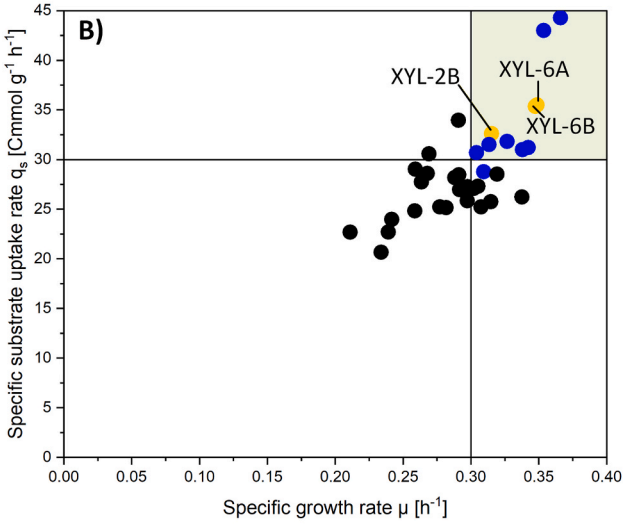

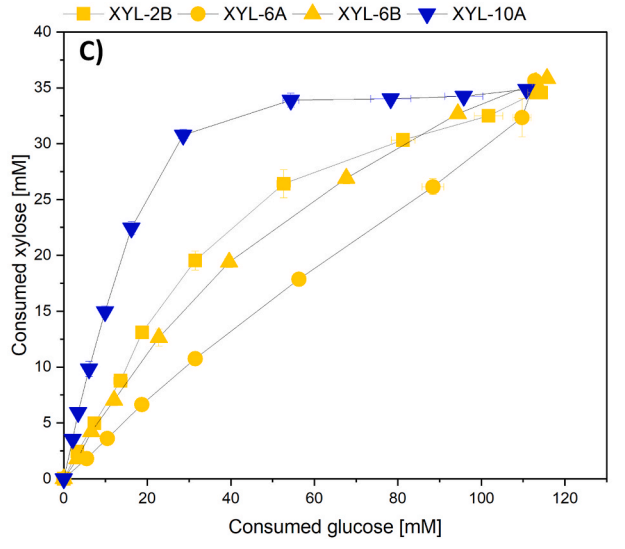

(caption on next column)

Fig. 6. Benchmarking of engineered *C. glutamicum* strains. (A) Specific growth rate (μ) versus co-utilization ratio (CUR). (B) Specific growth rate (μ) versus specific carbon-uptake rate (q_S, C-mmol g^{-1} h^{-1}). (C) Dynamics of the co-utilization ratio. Thresholds: $\mu \geq 0.30$ h^{-1}; CUR $\geq$0.30 mol mol^{-1}; $q_S \geq 30$ C-mmol g^{-1} h^{-1}. XYL-2B, XYL-6A, and XYL-6B meet all benchmarks (yellow). Data are means ± s.d. (biological triplicates). (For interpretation of the references to colour in this figure legend, the reader is referred to the Web version of this article.)

term redox or oxygen limitation (Wittmann et al., 2003). Cultures grown on CBH ultimately reached higher final biomass concentrations than those on defined sugar mixtures, consistent with the additional carbon and energy contributed by organic acid metabolism. Together, these results demonstrate that the engineered co-utilization phenotypes are robust and transferable to complex, waste-derived feedstocks. The top-performing variants—particularly XYL-6A and XYL-6B—combine balanced substrate assimilation, high metabolic throughput, and tolerance to secondary carbon sources, defining efficient chassis candidates for industrial bioprocesses based on mixed-sugar streams.

3.8. Performance of top strains across variable sugar mixtures

Because lignocellulosic and paper-waste-derived feedstocks display variable glucose:xylose ratios (Fig. 1), the three benchmark strains—XYL-2B, XYL-6A, and XYL-6B—were evaluated in defined sugar mixtures ranging from 100% glucose to 100% xylose in 25% increments (Fig. 8). The transporter-engineered strain XYL-10A was included as an additional comparator due to its unusually high CUR >1 and intrinsic xylose preference, which could provide an advantage in xylose-rich environments.

In glucose-only cultures, all strains reached stationary phase within approximately 13 h, exhibiting comparable growth kinetics. At a 3:1 glucose–xylose ratio, a positive auxiliary-substrate effect was observed, as all four strains grew faster in the mixed condition than on glucose alone. XYL-6A showed the strongest effect, shortening the time to stationary phase by 16% relative to the glucose-only control. As the xylose fraction increased, growth rates declined and lag phases extended across all strains; however, XYL-6A consistently maintained the highest specific growth rate under all conditions, including pure xylose.

In contrast, XYL-2B, XYL-6B, and XYL-10A exhibited disproportionately high CUR values, reflecting enhanced xylose uptake. For XYL-2B and XYL-6B, this led to reduced growth efficiency under xylose-rich conditions, likely due to an imbalance in central carbon flux distribution. XYL-10A, however, maintained robust growth even at high xylose proportions, confirming its capacity to sustain efficient metabolism under xylose-dominant conditions. This observation is consistent with its behavior in CBH fermentations, where XYL-10A showed slightly faster growth than in corresponding defined mixtures—suggesting a physiological advantage arising from its inherent xylose preference.

Although XYL-10A did not meet all substrate-informed performance benchmarks during CBH evaluation, its unique phenotype and stable growth across a wide range of substrate ratios identify it as a promising chassis for valorization of hydrolysates and mixed feedstocks with elevated xylose content. The results collectively underscore that efficient co-utilization depends not only on achieving balanced fluxes under idealized conditions but also on maintaining metabolic robustness across variable substrate compositions typical of industrial feedstocks.

3.9. Transcriptome analysis links co-utilization efficiency to transport regulation

To elucidate the molecular basis of efficient co-utilization, we analyzed the transcriptomic response of *C. glutamicum* XYL-6A across a gradient of glucose–xylose mixtures. Five conditions were examined—from 100% glucose to 100% xylose in 25% increments—using the glucose-only condition as the reference (Fig. 9). The number of

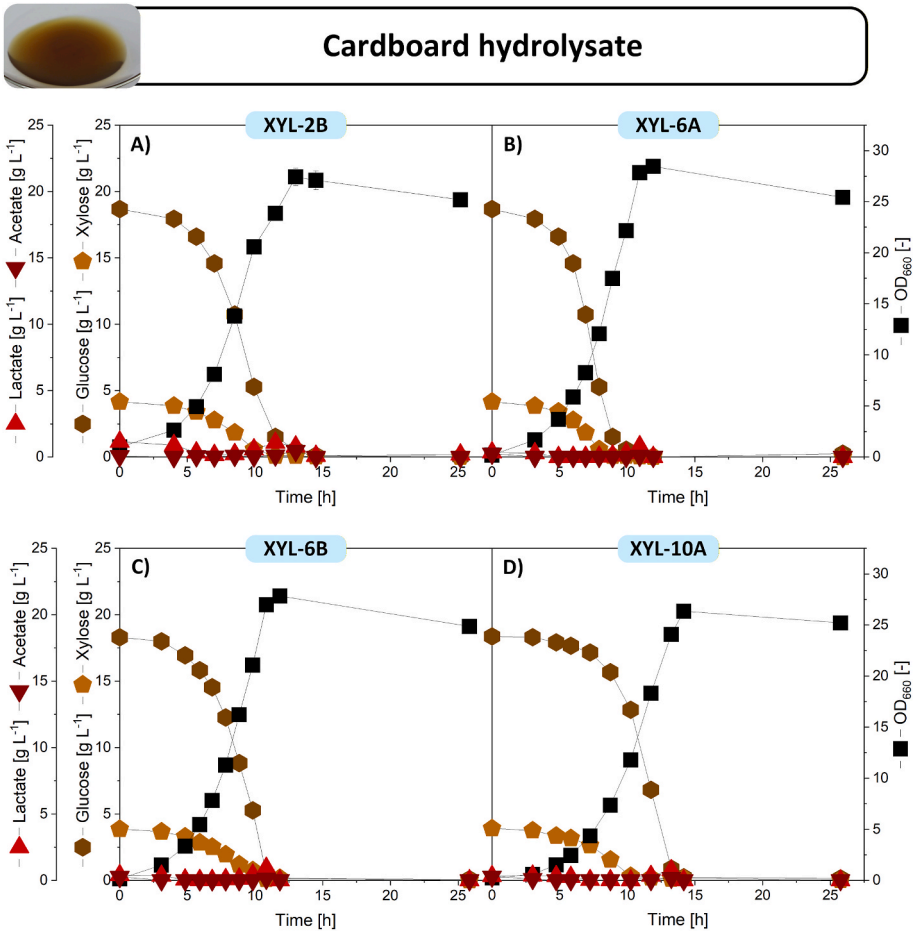

Fig. 7. Validation on cardboard hydrolysate (CBH). Strains XYL-2B, XYL-6A, XYL-6B, and XYL-10A were cultivated on 5% (v/v) CBH. In all cases, xylose was depleted in parallel with or prior to glucose. Lactate and acetate were co-consumed during exponential growth, transiently accumulated before stationary phase, and were fully depleted within 24 h. Data are means ± s.d. (biological triplicates).

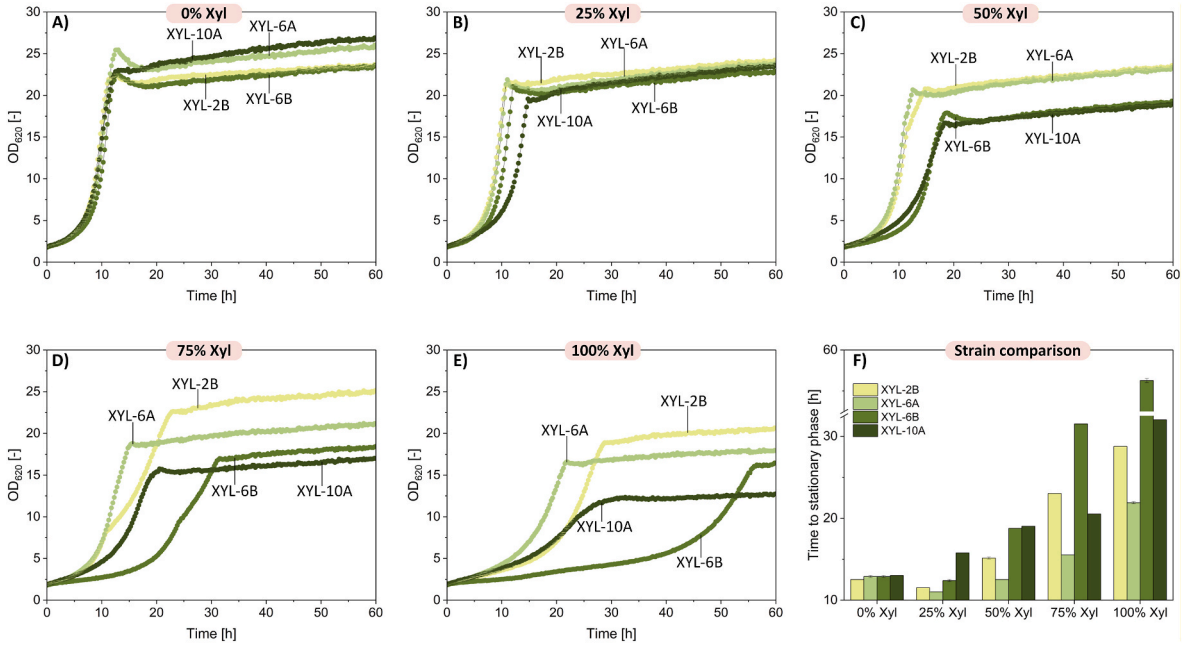

Fig. 8. Growth of benchmark strains across glucose–xylose ratios. XYL-2B, XYL-6A, XYL-6B, and XYL-10A were grown at total sugar 25 g L^{-1} with 0%, 25%, 50%, 75%, or 100% xylose. Panels A–E: growth profiles; (F) time to stationary phase. Data are means ± s.d. (biological duplicates).

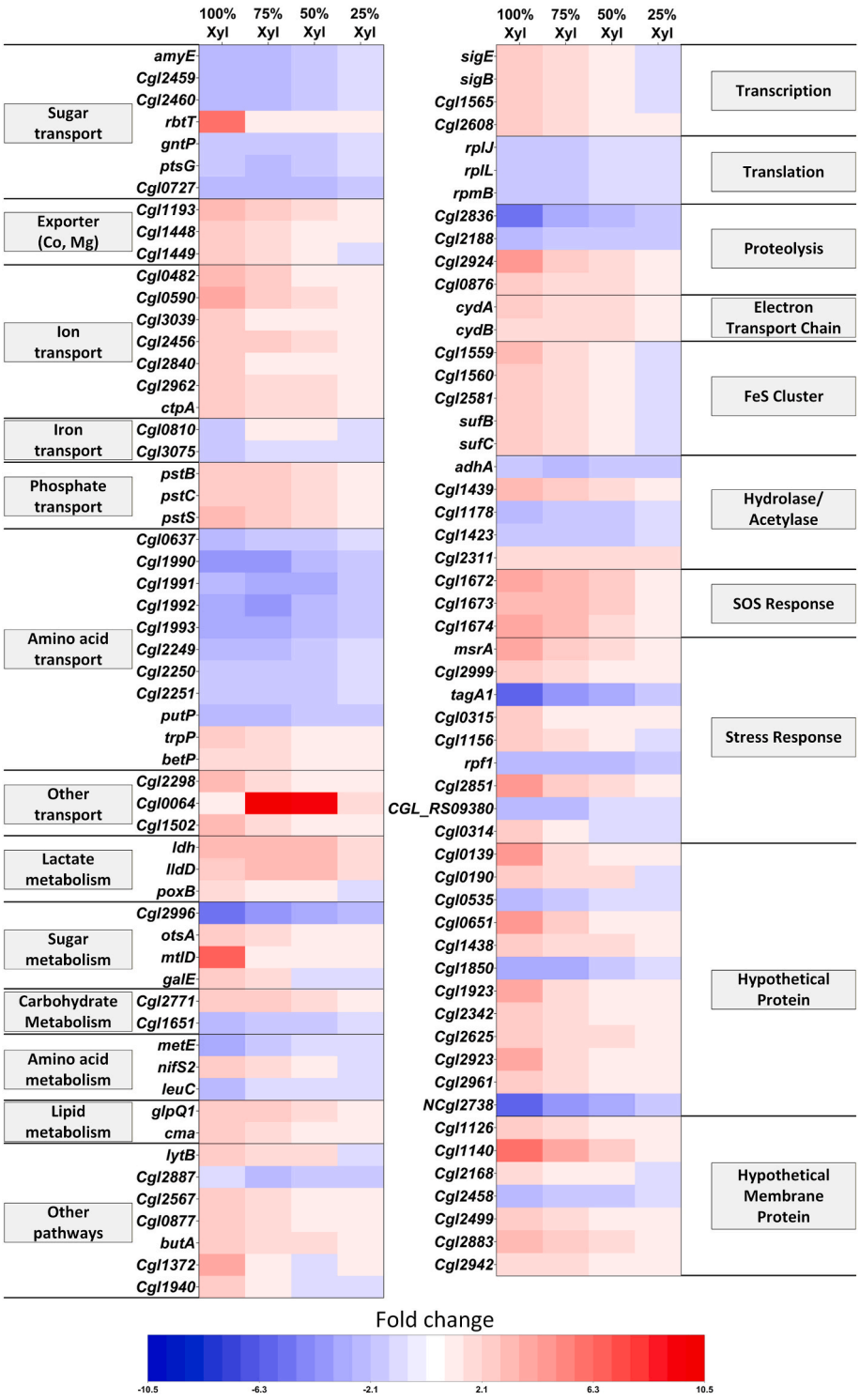

Fig. 9. Transcriptomic response of *C. glutamicum* XYL-6A to different glucose-xylose ratios. Gene expression in cultures with 25%, 50%, 75%, and 100% xylose relative to the glucose-only reference (0% xylose). Differentially expressed genes are grouped by function; upregulated genes in blue, downregulated in red. Means of biological triplicates. (For interpretation of the references to colour in this figure legend, the reader is referred to the Web version of this article.)

differentially expressed genes (DEGs) increased progressively with rising xylose fractions: 4 at 25% xylose, 18 at 50%, 53 at 75%, and 106 at 100% xylose. Apart from five genes uniquely regulated at intermediate mixtures, all DEGs detected at lower xylose levels were also affected at higher proportions. At 100% xylose, 69 genes were upregulated and 37 downregulated. Principal component analysis (PCA) showed clear separation of samples according to the glucose–xylose ratio while maintaining tight clustering within replicates, demonstrating high data quality and reproducibility (Fig. S12, Supplementary File 1).

The overall number of transcriptional changes was surprisingly low, considering the transition from a native substrate (glucose) to a non-native one (xylose). In other microorganisms, similar substrate shifts typically trigger hundreds to thousands of DEGs—for instance, *E. coli* exhibits more than 580 genes differentially expressed when switching between glucose and xylose (Gonzalez et al., 2002), *B. subtilis* responds to glucose-mediated catabolite repression via CcpA control of roughly

10% of its genome (Moreno et al., 2001), and *S. cerevisiae* reprograms approximately 30% of its genes during the diauxic shift from glucose to respiration (DeRisi et al., 1997). The minimal transcriptional response in XYL-6A is consistent with xylose being a non-native substrate in *C. glutamicum* and suggests that the heterologous *xylAB* pathway is only weakly integrated into endogenous transcriptional control networks. Accordingly, balanced glucose–xylose co-utilization appears to be maintained predominantly through metabolic and post-transcriptional mechanisms, rather than through extensive transcriptional remodeling.

Despite xylose being non-native to *C. glutamicum* ATCC 13032, genes of central carbon metabolism remained largely unaffected genes of central carbon metabolism remained largely unaffected, indicating that transcriptional regulation is unlikely to represent the dominant control layer for xylose flux under the conditions tested. This observation aligns with previous findings that metabolic enhancement of xylose utilization requires direct overexpression of pentose-phosphate pathway genes rather than global regulatory changes (Jo et al., 2017b). Instead, the transcriptional response was concentrated at the level of sugar transport. The glucose-specific (phosphotransferase system) PTS permease *ptsG* was downregulated, whereas the putative ribitol transporter *rbtT* was upregulated—changes indicative of adaptive substrate-uptake modulation rather than broad metabolic remodeling (Buschke et al., 2013; Engels et al., 2008). Overall, the transcriptomic response of XYL-6A was modest and largely confined to transporter-related genes, whereas core metabolic genes remained transcriptionally stable. The superior co-utilization phenotype of XYL-6A thus arises predominantly from engineered pathway balance and transporter activity, rather than from any glucose-dependent repression of the introduced xylose pathway.

This interpretation is supported by recent adaptive-laboratory-evolution studies in *C. glutamicum*, where improved glucose–xylose co-utilization correlated with *iolT2* upregulation (Ding et al., 2025) or *iolT1* mutation (Hofer et al., 2025), both affecting sugar transport. Together, these results emphasize that transport-level modulation, rather than global transcriptional rewiring, plays a dominant role in the system-level response during mixed-sugar utilization. Efficient co-utilization in *C. glutamicum* is therefore achieved through intrinsic network connectivity and post-transcriptional flux control—a design principle that can guide future metabolic-engineering strategies for stable, multi-substrate bioprocesses.

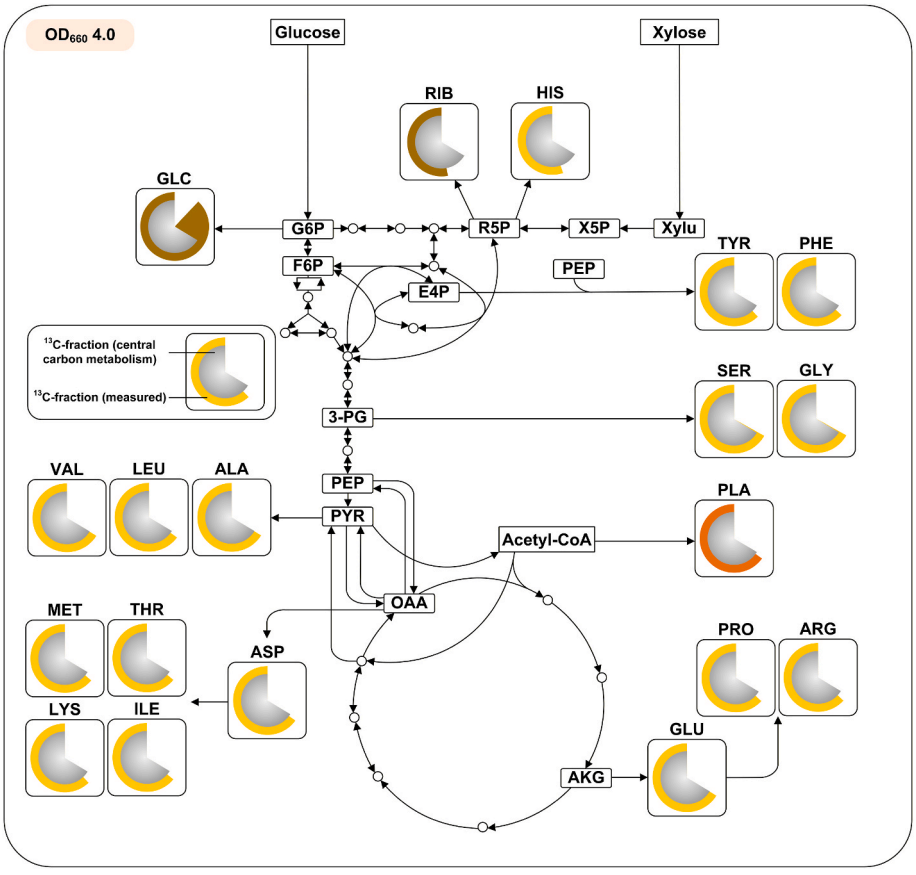

Fig. 10. ^{13}C-tracer labeling reveals balanced carbon convergence in *C. glutamicum* XYL-6A. Strain XYL-6A was cultivated in minimal medium containing 99 % [U-$^{13}C_6$] glucose and unlabelled xylose (4:1 ratio). Samples were taken during exponential growth (OD_{600} = 4.0) and analyzed for ^{13}C enrichment in proteinogenic amino acids, cellular sugars, and fatty acids using GC–MS. Pie charts display the relative ^{13}C enrichment, corresponding to the fraction of glucose-derived carbon (shown in yellow). Inner grey segments represent the theoretical fractions of glucose- and xylose-derived carbon anticipated from the measured substrate uptake ratios. Agreement between the outer (measured) and inner (expected) pies indicates complete and balanced carbon convergence. A higher ^{13}C enrichment than predicted reflects preferential incorporation of glucose-derived carbon, whereas lower enrichment indicates a relative increase in xylose contribution. ^{13}C-labeling patterns showed early and proportionally balanced flux convergence of glucose- and xylose-derived carbons at the F6P/G3P node, with substrate-specific isotopic signatures confined to the entry metabolites G6P, R5P, and E4P. Downstream carbon skeletons were fully merged, and minor dilution in TCA-cycle amino acids resulted from anaplerotic CO_2 fixation. The corresponding data set reflecting OD_{660} = 8.0 is given in Supplementary File 1. The persistence of these profiles across growth phases indicates a regulation-independent, kinetically balanced co-utilization regime. Means of biological triplicates. (For interpretation of the references to colour in this figure legend, the reader is referred to the Web version of this article.)

3.10. ^{13}C-tracer analysis reveals complete carbon convergence and pathway-specific substrate signatures in glucose–xylose-grown *C. glutamicum* XYL-6A

To elucidate intracellular carbon routing during glucose–xylose co-utilization, *C. glutamicum* XYL-6A was cultivated in minimal medium containing a mixture of 99% [U-$^{13}C_6$] glucose and unlabelled xylose, reflecting the 4:1 sugar ratio characteristic of cardboard hydrolysate. The purpose of the ^{13}C-tracer experiments was to assess the integration and stability of substrate-derived carbon fluxes under mixed-sugar conditions, rather than to determine absolute intracellular flux values by full ^{13}C metabolic flux analysis. Samples were collected during exponential growth (different time point, reflecting OD_{660} = 4.0 and 8.0) and analyzed for ^{13}C enrichment in proteinogenic amino acids, cellular sugars, and fatty acids using GC–MS (Fig. 10; Fig. S13, Supplementary File 1). Mass-isotopomer distributions were highly consistent at both sampling points. The stability of the labeling profiles indicates that glucose and xylose were co-utilized at a nearly constant ratio throughout growth.

To visualize carbon convergence, ^{13}C-enrichment data were displayed as pie charts (Fig. 10). The outer yellow segments represent the measured fraction of glucose-derived carbon, while the inner grey segments depict the theoretical glucose–xylose ratio inferred from substrate uptake. Close agreement between both indicates full convergence of glucose- and xylose-derived carbons; higher or lower ^{13}C enrichment denotes dominance of glucose- or xylose-derived flux, respectively.

Amino acids derived from 3-phosphoglycerate and pyruvate—serine, glycine, alanine, valine, and leucine—showed uniform ^{13}C enrichment (66-68 % SFL). Their glycolytic precursors, fructose 6-phosphate (F6P) and glyceraldehyde 3-phosphate (G3P), represent the key metabolic junction where glucose- and xylose-derived carbons converge via upper glycolysis and the non-oxidative pentose-phosphate (PP) pathway. These intermediates therefore reflect the merged metabolic mean of the central carbon flux.

Distinct substrate-specific isotopic signatures were confined to metabolites emerging directly from glucose 6-phosphate (G6P), ribose 5-phosphate (R5P), and to a lesser extent erythrose 4-phosphate (E4P). Cellular glucose, derived from G6P, was strongly labeled (88–90% SFL), confirming its glucose origin. By contrast, cellular ribose and histidine, originating from R5P, showed lower labeling (53–55% SFL and 9% below the glycolytic reference, respectively), demonstrating a significant contribution of xylose carbon through the pentose-phosphate pathway. Likewise, the aromatic amino acids tyrosine and phenylalanine—derived from E4P—displayed intermediate labeling levels (62–63%), consistent with a xylose-biased flux into the aromatic branch. The interpretation of these patterns is based on steady-state summed fractional labeling (SFL) comparisons between glycolytic and pentose-pathway-derived amino acids at two independent sampling points; while not a full metabolic-flux analysis, the consistency of SFL values within ≤3% across replicates supports functional mixing of the two carbon sources, as applied previously (Schwechheimer et al., 2018; Weiland et al., 2025).

Amino acids synthesized from tricarboxylic-acid (TCA) cycle intermediates—including aspartate, lysine, methionine, threonine, isoleucine, arginine, and proline—exhibited a modest 2–3% reduction in SFL relative to the glycolytic reference pool. This slight dilution results from anaplerotic carboxylation of pyruvate with unlabelled CO_2 (Yang et al., 2005), which introduces minor isotopic dilution into oxaloacetate and its derivatives rather than indicating incomplete substrate mixing (Krömer et al., 2004; Wittmann and Heinzle, 2001).

Collectively, the ^{13}C-labelling data reveal that carbon fluxes from glucose and xylose converge early and in a fixed proportion at the F6P/G3P node. While such convergence is an inherent property of central carbon metabolism, in strain XYL-6A it occurs quantitatively balanced and temporally stable, maintaining nearly constant flux ratios throughout growth. Substrate-specific isotopic signatures remained restricted to the immediate entry metabolites—G6P, R5P, and E4P—confirming complete mixing of carbon skeletons downstream of these nodes. Minor ^{13}C dilution within the TCA cycle originates solely from anaplerotic CO_2 -incorporation rather than incomplete substrate integration. The persistence of the labeling profiles across growth phases indicates a regulation-independent, kinetically balanced co-utilization regime, in which proportional flux partitioning arises from matched transporter and enzyme activities rather than transcriptional feedback. Because these interpretations derive from relative SFL patterns rather than full ^{13}C flux calculations, we describe the network behaviour as *functionally complete* convergence.

3.11. Lysine production from cardboard hydrolysate using the optimized xylose catabolic module

To evaluate the industrial relevance of the optimized co-utilization system, the *xylAB–xylE* cassette from strain XYL-6A was integrated into the lysine producer *C. glutamicum* LYS-12 (Becker et al., 2011), generating strain LYS-13 (Table 1). Shake-flask cultivations were conducted on both a defined 4:1 glucose–xylose mixture and on CBH as the sole carbon source (Fig. 11). Under both conditions, LYS-13 efficiently co-consumed xylose and glucose, with xylose depletion preceding glucose exhaustion. The strain achieved high lysine yields of 42.6 mmol C-mol^{-1} on the synthetic sugar mixture and 47.3 mmol C-mol^{-1} on CBH. These yields were comparable to, and in the case of CBH slightly higher than those of the parental LYS-12 strain cultivated on glucose alone (43 mmol C-mol^{-1}) (Becker et al., 2011).

These results confirm that the optimized co-utilization module integrates functionally into a production background without compromising flux efficiency. Xylose thereby contributes effectively to amino acid biosynthesis, while the slightly higher yield on CBH suggests minor components such as lactate and acetate may improve redox or cofactor balance.

4. Discussion

This study establishes a systematic, substrate-informed strain-engineering framework in *C. glutamicum* to overcome the long-standing challenge of stable glucose–xylose co-utilization. Previous efforts achieved partial co-utilization through transporter engineering, promoter modulation, or adaptive evolution (Buschke et al., 2011; Ding et al., 2025; Hofer et al., 2025; Yim et al., 2017), yet strains maintaining a near-constant co-utilization ratio and stable flux partitioning across growth phases and substrate conditions have remained rare. From a library of 34 engineered variants, we identified robust co-utilizers such as XYL-6A and XYL-6B that combined fast growth, balanced substrate use, and stable flux distribution independent of changing substrate levels. These phenotypes translated directly to CBH—a third-generation feedstock derived from non-recyclable paper waste—demonstrating that rational pathway design can deliver stable mixed-sugar metabolism under realistic industrial conditions. Several recent studies have demonstrated glucose–xylose co-utilization in *C. glutamicum* by introducing xylose assimilation pathways, identifying suitable transporters, or applying adaptive laboratory evolution (e.g. Ding et al., 2025). Building on these advances, the present work addresses a distinct and complementary layer of the co-utilization problem, namely the rational design of a kinetically stabilized flux regime in which relative substrate uptake rates remain invariant across time, substrate composition, and feedstock complexity.

A central finding of this study is that balanced glucose–xylose co-utilization is not a generic consequence of enabling xylose metabolism but emerges only within a narrow design window defined by the matching of transporter capacity and intracellular pathway kinetics. This conclusion is supported by the systematic analysis of 34 engineered variants, the majority of which display glucose-dominant uptake, diauxic behavior, or pronounced xylose preference. Only strains such as

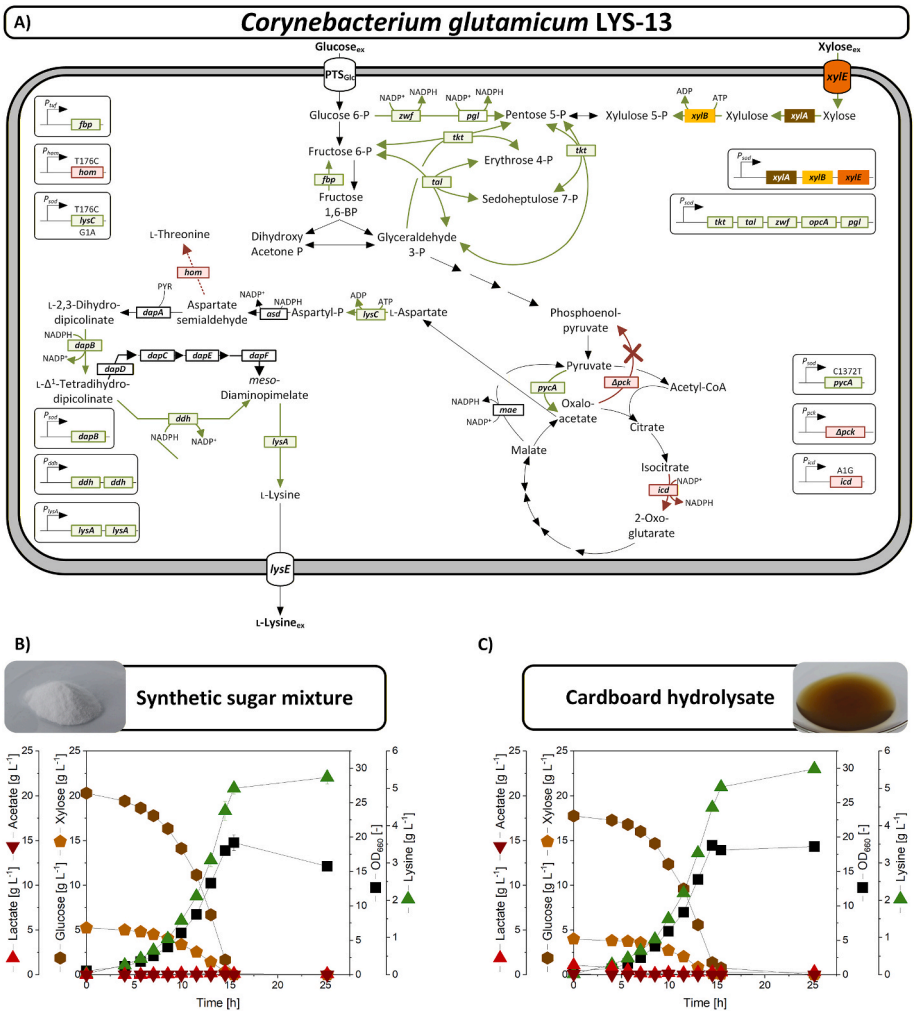

Fig. 11. Lysine production by *C. glutamicum* LYS-13. Minimal medium with (A) 20 g L^{-1} glucose + 5 g L^{-1} xylose or (B) 5% (v/v) CBH. Data are means ± s.d. (biological triplicates).

XYL-6A/B reproducibly exhibit temporally stable, fixed-ratio glucose–xylose uptake across defined sugar mixtures and cardboard hydrolysate. The strong phenotype selectivity observed across the strain library argues against a coincidental origin and instead indicates deliberate kinetic balancing as the dominant control principle.

Mechanistically, this regime is characterized by early convergence of glucose- and xylose-derived carbons at the fructose-6-phosphate/glyceraldehyde-3-phosphate node, forming a shared central-metabolic pool that stabilizes flux partitioning despite changing extracellular substrate levels. Transcriptome analysis reveals only limited transcriptional remodeling of central metabolism, with regulation occurring primarily at the level of transport-associated genes. Accordingly, we refer to this behavior as largely transcription-independent at the level of central carbon metabolism, with flux control dominated by transport and enzyme kinetics rather than global transcriptional reprogramming.

4.1. Novelty and industrial significance

Microbial valorization of lignocellulosic and paper-derived feedstocks has been hindered by glucose-dominant metabolism (Kim et al., 2010; Lynd et al., 2005). In *C. glutamicum*, introduction of *xylAB* enabled xylose catabolism (Buschke et al., 2011; Kawaguchi et al., 2006), and subsequent work improved this through transporter engineering (Werner et al., 2023; Yim et al., 2016), gene dosage variation (Sasaki et al., 2008), or adaptive evolution (Ding et al., 2025; Hofer et al., 2025). However, most of these studies were performed on defined sugar mixtures rather than realistic industrial substrates. CBH—containing glucose and xylose in a consistent 4:1 ratio (Kinnarinen et al., 2012b; Rauzi and Tschirner, 2022) along with organic acids (Jönsson and Martín, 2016; Palmqvist and Hahn-Hägerdal, 2000)—is a widely available but underutilized carbon source. With millions of tons generated annually in Europe (Eurostat, 2024), and mostly managed via incineration or landfilling (Belle et al., 2024), CBH represents an ideal target for circular-economy valorization. By aligning strain development directly with this substrate composition, the present study bridges rational metabolic design and process relevance, identifying generalist-type co-utilizers that maintain metabolic balance without external feeding control. Importantly, cardboard hydrolysate inherently contains organic acids such as acetate and lactate at inhibitory concentrations, and the stable co-utilization and growth observed in this medium therefore demonstrate the intrinsic robustness of the engineered strains under realistic process conditions.

Several strategies have been reported to enable glucose–xylose co-utilization in *Corynebacterium glutamicum*, including adaptive laboratory evolution and targeted regulatory modulation approaches such as CRISPRi (Ding et al., 2025; Hofer et al., 2025). These methods primarily act on transcriptional and regulatory layers and can yield effective phenotypes under specific conditions. In contrast, the substrate-informed strategy presented here targets kinetic balancing and flux integration at the level of central metabolism, resulting in stable co-utilization ratios that are maintained across growth phases, substrate compositions, and complex feedstocks. Importantly, these approaches

should be viewed as complementary rather than competing, as regulatory or evolutionary optimization could further refine strains built on a kinetically stabilized metabolic framework.

4.2. Fine-tuned cell factories: generalists and specialists

While *xylAB* and *xylE* from *E. coli* had been applied individually before (Buschke et al., 2011; Kim et al., 2010), their coordinated expression under a tuned promoter—as achieved in XYL-6A—yielded a balanced "generalist" strain that combined rapid growth, efficient co-utilization, and robust CBH performance. The superior behavior of XYL-6A illustrates the benefit of moderated gene expression in *C. glutamicum*: excessive transcription can impose translational burden and disrupt enzyme balance (Becker et al., 2005), whereas moderate expression aligns enzyme supply with pathway demand and avoids toxic intermediate buildup. This promoter-dependent control of pathway balance proved critical for integrating xylose catabolism with native glycolysis, supporting true co-utilization rather than sequential substrate use. While quantitative kinetic characterization of individual transporters would provide additional mechanistic resolution, the present analysis deliberately focuses on system-level uptake behavior under physiological conditions, which is most relevant for strain and process design.

A conceptually distinct "specialist" phenotype emerged later in strain XYL-10A, which displayed a xylose-preferential uptake pattern (CUR >1.0). To our knowledge, this represents a rare inversion of substrate hierarchy in *C. glutamicum* under defined laboratory conditions—given the near-universality of glucose dominance (Deutscher et al., 2006). Although growth rates were modestly lower, the discovery of a xylose-first phenotype broadens the design space for pentose-rich feedstocks such as hardwood hydrolysates (Larsson et al., 1999; Van Dyk and Pletschke, 2012), sugarcane bagasse (Canilha et al., 2012), and agricultural residues (Rumbold et al., 2009), strengthening the applicability of *C. glutamicum* to diverse feedstocks (Lira-Parada et al., 2022). The emergence of this phenotype is most plausibly attributed to transport- and pathway-level effects, including the use of the heterologous AraE symporter and the specific promoter configuration driving xylose uptake and phosphorylation, which together are expected to alter substrate competition at the uptake level. Further dissection of the relative contributions of transporter expression and promoter architecture, for example through targeted promoter-swapping experiments, would provide additional mechanistic resolution and represents an interesting direction for future work. Future optimization could pair this phenotype with enhanced PP pathway flux or NADPH regeneration to produce next-generation xylose-specialist producers.

4.3. Adaptability across substrate blends and translation to lysine production

Benchmarking across varying glucose–xylose ratios confirmed the broad adaptability of the engineered strains. XYL-6A maintained the highest growth rates across all substrate compositions, while XYL-10A, with its xylose-preferential phenotype, remained robust under xylose-rich conditions. Growth yields of XYL-10A were within ±5% of balanced co-utilizers, suggesting no significant energetic penalty associated with AraE-mediated proton symport under the tested conditions. This diversity of phenotypes—ranging from balanced co-utilizers to pentose specialists—illustrates the versatility of *C. glutamicum* as a modular host for valorization of heterogeneous carbohydrate feedstocks.

The transfer of the optimized xylose module into the industrial lysine producer LYS-12 (Becker et al., 2011) further demonstrated translational compatibility. The resulting strain, LYS-13, achieved lysine yields comparable to or exceeding those obtained on glucose alone (42.6 mmol C·mol^{-1} on synthetic mixtures and 47.3 mmol C·mol^{-1} on CBH). Despite only 25% of carbon in CBH originating from xylose, the substrate contributed substantially to lysine biosynthesis, demonstrating successful metabolic integration. Importantly, this performance was reached without extensive host adaptation or central metabolic rewiring, underscoring that the co-utilization module integrates functionally within a heavily optimized production chassis. Because the module stabilizes carbon flux partitioning at the level of central metabolism, its applicability is not restricted to lysine biosynthesis but is expected to extend broadly across different product pathways. Accordingly, these findings establish a platform for expanding amino acid and derivative production from xylose-containing waste feedstocks, a long-standing challenge in industrial biotechnology (Gopinath et al., 2011; Jin and Bao, 2021; Jo et al., 2017b; Meiswinkel et al., 2013). Beyond lysine, this design can be extended to other lysine-derived products such as diaminopentane (Kind et al., 2014), L-pipecolic acid (Pauli et al., 2023), ectoine (Giesselmann et al., 2019), hydroxyectoine (Jungmann et al., 2022), 5-aminovalerate (Rohles et al., 2022), and glutarate (Rohles et al., 2018). While the present study focuses on batch conditions, the kinetic balancing principles identified here are expected to be directly relevant under fed-batch operation, where stable substrate co-utilization can reduce the need for complex feeding strategies; dedicated fed-batch validation will be an important focus of future work.

4.4. Mechanistic basis of co-utilization

Transcriptomic and ^{13}C-tracer analyses provided complementary insights into how balanced glucose–xylose metabolism is achieved. The global transcriptional response of XYL-6A to xylose was remarkably limited—only 106 genes were differentially expressed under 100% xylose—substantially fewer than typically observed in other microorganisms during carbon-source transitions. This likely reflects the absence of evolved xylose-specific regulatory systems in *C. glutamicum*, which instead relies on constitutive metabolic flexibility. In contrast, *E. coli*, *B. subtilis*, and *S. cerevisiae* undergo extensive transcriptome remodeling when switching carbon sources, involving hundreds to thousands of genes (DeRisi et al., 1997; Gonzalez et al., 2002; Moreno et al., 2001). The minimal response observed here therefore suggests that balanced co-utilization in *C. glutamicum* is primarily governed by metabolic and post-transcriptional mechanisms rather than transcriptional reprogramming. Microarray sensitivity limits the detection of subtle (<1.3-fold) transcriptional changes. Although *C. glutamicum* can exhibit pathway-specific glucose repression, recently shown for aromatic catabolism (Weiland et al., 2025), these regulatory circuits do not apply to xylose, which lacks a native catabolic route in this organism. Thus, we interpret the 'minimal response' as few genes meeting differential-expression thresholds, not as a complete absence of regulation.

Consistent with this view, regulation in XYL-6A was concentrated at the transport level. The glucose-specific PTS permease *ptsG* was downregulated, whereas the putative ribitol transporter *rbtT* was upregulated—changes indicative of adaptive substrate uptake modulation rather than broad metabolic remodeling (Engels and Wendisch, 2007). At the same time, the putative ribitol transporter *rbtT* was induced, suggesting an auxiliary role in xylose uptake, as previously observed during heterologous xylose metabolism (Buschke et al., 2013). The coordinated downregulation of the glucose-specific PTS component ptsG and upregulation of rbtT likely contribute to reduced glucose dominance at the uptake level, thereby facilitating balanced entry of glucose- and xylose-derived carbon into central metabolism. Similar transporter-level adjustments were reported in ALE-derived strains where *iolT1* mutations and *iolT2* upregulation enhanced xylose uptake (Ding et al., 2025; Hofer et al., 2025). These consistent observations highlight transporter regulation as a dominant mechanism for establishing balanced substrate utilization in *C. glutamicum*.

The ^{13}C-labeling data reinforce this mechanistic interpretation by demonstrating complete carbon convergence at the F6P/G3P node within the resolution of SFL-based isotopomer analysis, similar to

growth on sucrose that is cleaved intracellularly into its two hexose monomers which are then metabolized through fully merged fluxes (Lange et al., 2017; Wittmann et al., 2004). While such convergence is a universal feature of central carbon metabolism, the distinguishing feature in strain XYL-6A was the timing and proportionality of this merge. Rather than sequential or imbalanced flux entry—as commonly observed under carbon catabolite repression—the glucose- and xylose-derived fluxes in XYL-6A converged early and in fixed proportion, maintaining a constant ratio across growth phases. This defines a distinct, regulation-independent metabolic regime in which balanced carbon integration arises from kinetic matching of transporter and enzyme capacities rather than from transcriptional control. In this state, substrate fluxes are co-channeled into the F6P/G3P node at steady relative rates, generating a stable and self-balanced network behavior that contrasts with the dynamic repression–relief cycles typical of canonical co-utilization systems.

Substrate-specific isotopic signatures were confined to the immediate entry points of glucose and xylose—G6P, R5P, and E4P—while all downstream metabolites, including amino acids derived from glycolysis and the TCA cycle, exhibited fully merged labeling patterns (Mutz et al., 2024). These patterns indicate functional flux merging downstream of the F6P/G3P node, although SFL does not quantify absolute fluxes. The constancy of these isotopic distributions across growth phases indicates that *C. glutamicum* maintains a temporally stable flux ratio between glucose and xylose, independent of absolute substrate concentrations. This behavior reflects a self-regulating metabolic network in which flux balance arises intrinsically from pathway connectivity and enzyme-level control rather than dynamic transcriptional feedback.

Building on our observations, the flux regime identified in strain XYL-6A points to a mixed-sugar metabolism that is mechanistically distinct from previously reported xylose-utilizing *C. glutamicum* strains. Unlike earlier studies that merely enabled xylose catabolism or mitigated substrate hierarchy through pathway introduction or evolution (Ding et al., 2025; Hofer et al., 2025; Yim et al., 2017), XYL-6A achieves quantitatively balanced co-utilization through kinetic coordination of uptake and pathway enzyme activities. This regime establishes an early and fixed-proportion carbon convergence at the F6P/G3P node that remains robust without transcriptional adaptation. Such largely transcription-independent flux integration illustrates a generalizable design principle: balanced transporter and enzyme capacities can create self-stabilizing co-utilization states, providing a mechanistic framework for rational engineering of other mixed-substrate bioprocesses.

Within this framework, the choice of xylose catabolic route is central. The isomerase pathway used here is redox neutral and feeds directly into xylulose-5-phosphate, integrating naturally with the PP pathway that supports precursor and NADPH supply in amino-acid production. By contrast, oxidoreductase, Dahms, or Weimberg routes alter redox balance or divert carbon to metabolic nodes downstream of the upper PP pathway, typically requiring broader network rewiring to achieve similar flux balance (Domingues et al., 2021; Jo et al., 2017a). The compact xylA/xylB module therefore provides a particularly compatible basis for establishing the balanced co-utilization regime observed in XYL-6A. Full ^{13}C metabolic flux analysis using multiple tracers would provide quantitative resolution of intracellular flux distributions and represents an important direction for future work building on the design principles established here.

At the enzyme level, the xylose isomerase pathway is governed by straightforward kinetic features. XylA and XylB lack dedicated allosteric control and respond primarily to divalent ions and mild product inhibition (Bunker et al., 2013; Lee et al., 2017), while oxidative PP pathway enzymes are regulated mainly by the intracellular NADPH/$NADP^+$ ratio (Stanton, 2012). These simple dependencies are fully consistent with the limited transcriptomic response, reinforcing that stable glucose–xylose co-utilization in XYL-6A is maintained through intrinsic enzyme properties and metabolic connectivity rather than transcriptional control. Transcriptome analysis of additional genetic backgrounds, including strains lacking heterologous transporter overexpression, would be a valuable direction for future work to further disentangle native versus engineered transport contributions.

5. Summary and outlook

This study establishes *C. glutamicum* as an efficient host for simultaneous glucose–xylose co-utilization and sustainable bioproduction from CBH. Through systematic, substrate-informed engineering of 34 strain variants, we developed modular xylose catabolic systems that achieve balanced, largely transcription-independent co-utilization at the level of central carbon metabolism and translate effectively into an industrial lysine producer. These results demonstrate that pathway and transporter tuning alone can overcome carbon catabolite repression and enable robust mixed-sugar metabolism under realistic feedstock conditions.

A key advantage of this regime is that it emerges without targeted suppression of native glucose uptake, extensive pathway amplification, or specialized feeding strategies. Instead, balanced glucose–xylose fluxes arise from the inherent kinetics of a compact, redox-neutral isomerase pathway combined with calibrated transporter capacities. This minimal interference with central metabolism reduces metabolic burden and ensures stable performance across conditions. Together, these features exemplify a central synthetic-biology principle—simple, robust and scalable designs can achieve complex metabolic behaviours without elaborate regulatory rewiring—and provide a practical foundation for mixed-sugar bioprocessing under industrially relevant conditions.

Beyond the biological advance, the industrial potential of CBH underscores the significance of this work. In the EU, approximately 34 Mt of paper and cardboard packaging waste are generated annually, of which an estimated 5.8 Mt remain unrecycled despite high collection efficiencies (Eurostat, 2024). Based on reported hydrolysis yields, this fraction represents roughly 1.0–2.3 Mt of fermentable sugars each year (Rauzi and Tschirner, 2022)—equivalent to 4–6 million m^3 of concentrated, process-ready feedstock at typical hydrolysate concentrations (300–400 g L^{-1} sugars). This volume corresponds to the carbon input required for multiple world-scale amino acid or organic acid fermentations, highlighting unrecyclable cardboard as a substantial yet untapped resource within the circular bioeconomy.

The demonstrated robustness of our engineered *C. glutamicum* strains on CBH, together with their successful integration into an industrial production host, provides a solid foundation for translating this feedstock into practice. By linking mechanistic understanding of flux integration to scalable process performance, this work exemplifies how rational pathway design can convert residual carbon streams into sustainable, high-value bioproducts and advance the transition toward resource-efficient biomanufacturing.

CRediT authorship contribution statement

David J. Mees: Writing – review & editing, Writing – original draft, Visualization, Methodology, Investigation, Data curation, Conceptualization. **Peng Cao:** Writing – review & editing, Methodology, Investigation, Data curation. **Ann-Kathrin Thönes:** Writing – review & editing, Methodology. **Mario V. Ternes:** Writing – review & editing, Methodology. **Michael Kohlstedt:** Writing – review & editing, Methodology, Investigation, Data curation. **Christoph Wittmann:** Writing – review & editing, Writing – original draft, Visualization, Supervision, Resources, Project administration, Funding acquisition, Data curation, Conceptualization.

Declarations of competing interest

The authors declare that they have no conflicts of interest.

Acknowledgements

This project has received funding from the European Union's Horizon Europe Program under Grant Agreement number: 101057971. Open-access funding was provided and organized by Projekt DEAL. The authors acknowledge the excellent assistance of Michel Fritz in analytics.

Appendix A. Supplementary data

Supplementary data to this article can be found online at https://doi.org/10.1016/j.ymben.2026.02.007.

Data availability

Data will be made available on request.

References

Becker, J., Buschke, N., Bücker, R., Wittmann, C., 2010. Systems Level Engineering of *Corynebacterium glutamicum* – Reprogramming Translational Efficiency for Superior Production, 10. Engineering in Life Sciences, pp. 430–438.

Becker, J., Klopprogge, C., Herold, A., Zelder, O., Bolten, C.J., Wittmann, C., 2007. Metabolic flux engineering of L-lysine production in *Corynebacterium glutamicum*–over expression and modification of G6P dehydrogenase. J. Biotechnol. 132, 99–109.

Becker, J., Klopprogge, C., Zelder, O., Heinzle, E., Wittmann, C., 2005. Amplified expression of fructose 1,6-bisphosphatase in *Corynebacterium glutamicum* increases *in vivo* flux through the pentose phosphate pathway and lysine production on different carbon sources. Appl. Environ. Microbiol. 71, 8587–8596.

Becker, J., Kuhl, M., Kohlstedt, M., Starck, S., Wittmann, C., 2018. Metabolic engineering of *Corynebacterium glutamicum* for the production of *cis, cis*-muconic acid from lignin. Microb. Cell Fact. 17, 115.

Becker, J., Zelder, O., Haefner, S., Schröder, H., Wittmann, C., 2011. From zero to hero–design-based systems metabolic engineering of *Corynebacterium glutamicum* for L-lysine production. Metab. Eng. 13, 159–168.

Belle, J., Hirtz, D., Sängerlaub, S., 2024. Expert survey on the impact of cardboard and paper recycling processes, fiber-based composites/laminates and regulations, and their significance for the circular economy and the sustainability of the German paper industry. Sustainability 16, 6610.

Blombach, B., Seibold, G.M., 2010. Carbohydrate metabolism in *Corynebacterium glutamicum* and applications for the metabolic engineering of L-lysine production strains. Appl. Microbiol. Biotechnol. 86, 1313–1322.

Brat, D., Boles, E., Wiedemann, B., 2009. Functional expression of a bacterial xylose isomerase in *Saccharomyces cerevisiae*. Appl. Environ. Microbiol. 75, 2304–2311.

Bunker, R.D., Bulloch, E.M., Dickson, J.M., Loomes, K.M., Baker, E.N., 2013. Structure and function of human xylulokinase, an enzyme with important roles in carbohydrate metabolism. J. Biol. Chem. 288, 1643–1652.

Buschke, N., Becker, J., Schäfer, R., Kiefer, P., Biedendieck, R., Wittmann, C., 2013. Systems metabolic engineering of xylose-utilizing *Corynebacterium glutamicum* for production of 1,5-diaminopentane. Biotechnol. J. 8, 557–570.

Buschke, N., Schröder, H., Wittmann, C., 2011. Metabolic engineering of *Corynebacterium glutamicum* for production of 1,5-diaminopentane from hemicellulose. Biotechnol. J. 6, 306–317.

Canilha, L., Chandel, A.K., Suzane dos Santos Milessi, T., Antunes, F.A.F., Luiz da Costa Freitas, W., das Graças Almeida Felipe, M., da Silva, S.S., 2012. Bioconversion of sugarcane biomass into ethanol: an overview about composition, pretreatment methods, detoxification of hydrolysates, enzymatic saccharification, and ethanol fermentation. BioMed Res. Int. 2012, 989572.

Chen, Z., Huang, J.H., Wu, Y., Wu, W.J., Zhang, Y., Liu, D.H., 2017. Metabolic engineering of *Corynebacterium glutamicum* for the production of 3-hydroxypropionic acid from glucose and xylose. Metab. Eng. 39, 151–158.

Christmann, J., Cao, P., Becker, J., Desiderato, C.K., Goldbeck, O., Riedel, C.U., Kohlstedt, M., Wittmann, C., 2023. High-efficiency production of the antimicrobial peptide pediocin PA-1 in metabolically engineered *Corynebacterium glutamicum* using a microaerobic process at acidic pH and elevated levels of bivalent calcium ions. Microb. Cell Fact. 22, 41.

Demeke, M.M., Dietz, H., Li, Y., Foulquie-Moreno, M.R., Mutturi, S., Deprez, S., Den Abt, T., Bonini, B.M., Liden, G., Dumortier, F., Verplaetse, A., Boles, E., Thevelein, J. M., 2013. Development of a D-xylose fermenting and inhibitor tolerant industrial *Saccharomyces cerevisiae* strain with high performance in lignocellulose hydrolysates using metabolic and evolutionary engineering. Biotechnol. Biofuels 6, 89.

DeRisi, J.L., Iyer, V.R., Brown, P.O., 1997. Exploring the metabolic and genetic control of gene expression on a genomic scale. Science 278, 680–686.

Deutscher, J., Francke, C., Postma, P.W., 2006. How phosphotransferase system-related protein phosphorylation regulates carbohydrate metabolism in bacteria. Microbiol. Mol. Biol. Rev. 70, 939–1031.

Dietrich, D., Jovanovic-Gasovic, S., Cao, P., Kohlstedt, M., Wittmann, C., 2023. Refactoring the architecture of a polyketide gene cluster enhances docosahexaenoic acid production in *Yarrowia lipolytica* through improved expression and genetic stability. Microb. Cell Fact. 22.

Ding, N., Yan, J., Luo, Q., Chen, H., Qin, Y., Ye, J., Tian, K., Shao, Q., Volkov, P.V., Liang, R., Deng, Y., Yin, L., 2025. Engineering xylose metabolism and coutilization with glucose in *Corynebacterium glutamicum* for efficient microbial cell factories. J. Agric. Food Chem. 73, 19587–19598.

Domingues, R., Bondar, M., Palolo, I., Queirós, O., de Almeida, C.D., Cesário, M.T., 2021. Xylose metabolism in bacteria—opportunities and challenges towards efficient lignocellulosic biomass-based biorefineries. Appl. Sci. 11, 8112.

Eliasson, A., Christensson, C., Wahlbom, C.F., Hahn-Hägerdal, B., 2000. Anaerobic xylose fermentation by recombinant *Saccharomyces cerevisiae* carrying *XYL1, XYL2*, and *XKS1* in mineral medium chemostat cultures. Appl. Environ. Microbiol. 66, 3381–3386.

Engels, V., Lindner, S.N., Wendisch, V.F., 2008. The global repressor SugR controls expression of genes of glycolysis and of the L-lactate dehydrogenase LdhA in *Corynebacterium glutamicum*. J. Bacteriol. 190, 8033–8044.

Engels, V., Wendisch, V.F., 2007. The DeoR-type regulator SugR represses expression of ptsG in *Corynebacterium glutamicum*. J. Bacteriol. 189, 2955–2966.

Eurostat, Packaging, 2024. Waste statistics. Eurostat Statist. Explain. 2025.

Fonseca, C., Olofsson, K., Ferreira, C., Runquist, D., Fonseca, L.L., Hahn-Hägerdal, B., Lidén, G., 2011. The glucose/xylose facilitator Gxf1 from *Candida intermedia* expressed in a xylose-fermenting industrial strain of *Saccharomyces cerevisiae* increases xylose uptake in SSCF of wheat straw. Enzym. Microb. Technol. 48, 518–525.

Gancedo Juana, M., 1998. Yeast carbon catabolite repression. Microbiol. Mol. Biol. Rev. 62, 334–361.

Gao, Q., Zhang, M., McMillan, J.D., Kompala, D.S., 2002. Characterization of heterologous and native enzyme activity profiles in metabolically engineered *Zymomonas mobilis* strains during batch fermentation of glucose and xylose mixtures. Appl. Biochem. Biotechnol. 98, 341–355.

Gárdonyi, M., Jeppsson, M., Lidén, G., Gorwa-Grauslund, M.F., Hahn-Hägerdal, B., 2003. Control of xylose consumption by xylose transport in recombinant *Saccharomyces cerevisiae*. Biotechnol. Bioeng. 82, 818–824.

Gibson, D.G., Young, L., Chuang, R.Y., Venter, J.C., Hutchison 3rd, C.A., Smith, H.O., 2009. Enzymatic assembly of DNA molecules up to several hundred kilobases. Nat. Methods 6, 343–345.

Giesselmann, G., Dietrich, D., Jungmann, L., Kohlstedt, M., Jeon, E.J., Yim, S.S., Sommer, F., Zimmer, D., Mühlhaus, T., Schroda, M., Jeong, K.J., Becker, J., Wittmann, C., 2019. Metabolic engineering of *Corynebacterium glutamicum* for high-level ectoine production: design, combinatorial assembly, and implementation of a transcriptionally balanced heterologous ectoine pathway. Biotechnol. J. 14, e1800417.

Gonzalez, R., Tao, H., Shanmugam, K.T., York, S.W., Ingram, L.O., 2002. Global gene expression differences associated with changes in glycolytic flux and growth rate in Escherichia coli during the fermentation of glucose and xylose. Biotechnol. Prog. 18, 6–20.

Gopinath, V., Meiswinkel, T.M., Wendisch, V.F., Nampoothiri, K.M., 2011. Amino acid production from rice straw and wheat bran hydrolysates by recombinant pentose-utilizing *Corynebacterium glutamicum*. Appl. Microbiol. Biotechnol. 92, 985–996.

Hofer, K., Schwardmann, L.S., Youn, J.-W., Wendisch, V.F., Takors, R., 2025. Single mutation in *iolT1* in *ptsG*-deficient *Corynebacterium glutamicum* enables growth boost in xylose-containing media. Microorganisms 13, 1606.

Hoffmann, S.L., Jungmann, L., Schiefelbein, S., Peyriga, L., Cahoreau, E., Portais, J.C., Becker, J., Wittmann, C., 2018. Lysine production from the sugar alcohol mannitol: design of the cell factory *Corynebacterium glutamicum* SEA-3 through integrated analysis and engineering of metabolic pathway fluxes. Metab. Eng. 47, 475–487.

Ikeda, M., Nakagawa, S., 2003. The *Corynebacterium glutamicum* genome: features and impacts on biotechnological processes. Appl. Microbiol. Biotechnol. 62, 99–109.

Inoue, H., Nojima, H., Okayama, H., 1990. High efficiency transformation of *Escherichia coli* with plasmids. Gene 96, 23–28.

Jin, C., Bao, J., 2021. Lysine production by dry biorefining of wheat straw and cofermentation of *Corynebacterium glutamicum*. J. Agric. Food Chem. 69, 1900–1906.

Jo, S., Yoon, J., Lee, S.-M., Um, Y., Han, S.O., Woo, H.M., 2017a. Modular pathway engineering of *Corynebacterium glutamicum* to improve xylose utilization and succinate production. J. Biotechnol. 258, 69–78.

Jo, S., Yoon, J., Lee, S.M., Um, Y., Han, S.O., Woo, H.M., 2017b. Modular pathway engineering of *Corynebacterium glutamicum* to improve xylose utilization and succinate production. J. Biotechnol. 258, 69–78.

Jönsson, L.J., Martín, C., 2016. Pretreatment of lignocellulose: formation of inhibitory by-products and strategies for minimizing their effects. Bioresour. Technol. 199, 103–112.

Jungmann, L., Hoffmann, S.L., Lang, C., De Agazio, R., Becker, J., Kohlstedt, M., Wittmann, C., 2022. High-efficiency production of 5-hydroxyectoine using metabolically engineered *Corynebacterium glutamicum*. Microb. Cell Fact. 21, 274.

Kalinowski, J., Bathe, B., Bartels, D., Bischoff, N., Bott, M., Burkovski, A., Dusch, N., Eggeling, L., Eikmanns, B.J., Gaigalat, L., Goesmann, A., Hartmann, M., Huthmacher, K., Krämer, R., Linke, B., McHardy, A.C., Meyer, F., Möckel, B., Pfefferle, W., Pühler, A., Rey, D.A., Rückert, C., Rupp, O., Sahm, H., Wendisch, V.F., Wiegrabe, I., Tauch, A., 2003. The complete *Corynebacterium glutamicum* ATCC 13032 genome sequence and its impact on the production of L-aspartate-derived amino acids and vitamins. J. Biotechnol. 104, 5–25.

Kaplan Nicholas, A., Islam Khondokar, N., Kanis Fiona, C., Verderber Jack, R., Wang, X., Jones, J.A., Koffas Mattheos, A.G., 2024. Simultaneous glucose and xylose utilization by an *Escherichia coli* catabolite repression mutant. Appl. Environ. Microbiol. 90 e02169–23.

Kawaguchi, H., Vertes, A.A., Okino, S., Inui, M., Yukawa, H., 2006. Engineering of a xylose metabolic pathway in *Corynebacterium glutamicum*. Appl. Environ. Microbiol. 72, 3418–3428.

Kim, J.H., Block, D.E., Mills, D.A., 2010. Simultaneous consumption of pentose and hexose sugars: an optimal microbial phenotype for efficient fermentation of lignocellulosic biomass. Appl. Microbiol. Biotechnol. 88, 1077–1085.
Kim, J.H., Shoemaker, S.P., Mills, D.A., 2009. Relaxed control of sugar utilization in *Lactobacillus brevis*. Microbiology (Read.) 155, 1351–1359.
Kim, S.R., Ha, S.J., Wei, N., Oh, E.J., Jin, Y.S., 2012. Simultaneous co-fermentation of mixed sugars: a promising strategy for producing cellulosic ethanol. Trends Biotechnol. 30, 274–282.
Kind, S., Neubauer, S., Becker, J., Yamamoto, M., Völkert, M., Abendroth, G.V., Zelder, O., Wittmann, C., 2014. From zero to hero - production of bio-based nylon from renewable resources using engineered *Corynebacterium glutamicum*. Metab. Eng. 25, 113–123.
Kinnarinen, T., Huhtanen, M., Häkkinen, A., Louhi-Kultanen, M., 2012a. Solid-liquid separation of hydrolysates obtained from enzymatic hydrolysis of cardboard waste. Ind. Crop. Prod. 38, 72–80.
Kinnarinen, T., Shakhanova, M., Hietanen, E., Salmimies, R., Häkkinen, A., Louhi-Kultanen, M., 2012b. Effect of mixing on enzymatic hydrolysis of cardboard waste: saccharification yield and subsequent separation of the solid residue using a pressure filter. Bioresour. Technol. 110, 405–411.
Ko, J.K., Enkh-Amgalan, T., Gong, G., Um, Y., Lee, S.M., 2020. Improved bioconversion of lignocellulosic biomass by *Saccharomyces cerevisiae* engineered for tolerance to acetic acid. GCB Bioenergy 12, 90–100.
Ko, J.K., Um, Y., Woo, H.M., Kim, K.H., Lee, S.M., 2016. Ethanol production from lignocellulosic hydrolysates using engineered *Saccharomyces cerevisiae* harboring xylose isomerase-based pathway. Bioresour. Technol. 209, 290–296.
Kohlstedt, M., Sappa, P.K., Meyer, H., Maass, S., Zaprasis, A., Hoffmann, T., Becker, J., Steil, L., Hecker, M., van Dijl, J.M., Lalk, M., Mader, U., Stulke, J., Bremer, E., Volker, U., Wittmann, C., 2014. Adaptation of *Bacillus subtilis* carbon core metabolism to simultaneous nutrient limitation and osmotic challenge: a multi-omics perspective. Environ. Microbiol. 16, 1898–1917.
Kohlstedt, M., Starck, S., Barton, N., Stolzenberger, J., Selzer, M., Mehlmann, K., Schneider, R., Pleissner, D., Rinkel, J., Dickschat, J.S., Venus, J., J, B.J. H.v.D., Wittmann, C., 2018. From lignin to nylon: cascaded chemical and biochemical conversion using metabolically engineered *Pseudomonas putida*. Metab. Eng. 47, 279–293.
Kohlstedt, M., Weimer, A., Weiland, F., Stolzenberger, J., Selzer, M., Sanz, M., Kramps, L., Wittmann, C., 2022. Biobased PET from lignin using an engineered cis, cis-muconate-producing *Pseudomonas putida* strain with superior robustness, energy and redox properties. Metab. Eng. 72, 337–352.
Kohlstedt, M., Wittmann, C., 2019. GC-MS-based ^{13}C metabolic flux analysis resolves the parallel and cyclic glucose metabolism of *Pseudomonas putida* KT2440 and PAO1. Metab. Eng. 54, 35–53.
Krömer, J.O., Fritz, M., Heinzle, E., Wittmann, C., 2005. *In vivo* quantification of intracellular amino acids and intermediates of the methionine pathway in *Corynebacterium glutamicum*. Anal. Biochem. 340, 171–173.
Krömer, J.O., Sorgenfrei, O., Klopprogge, K., Heinzle, E., Wittmann, C., 2004. In-depth profiling of lysine-producing *Corynebacterium glutamicum* by combined analysis of the transcriptome, metabolome, and fluxome. J. Bacteriol. 186, 1769–1784.
Lange, A., Becker, J., Schulze, D., Cahoreau, E., Portais, J.C., Haefner, S., Schröder, H., Krawczyk, J., Zelder, O., Wittmann, C., 2017. Bio-based succinate from sucrose: high-resolution ^{13}C metabolic flux analysis and metabolic engineering of the rumen bacterium *Basfia succiniciproducens*. Metab. Eng. 44, 198–212.
Larsson, S., Reimann, A., Nilvebrant, N.-O., Jönsson, L.J., 1999. Comparison of different methods for the detoxification of lignocellulose hydrolyzates of spruce. Appl. Biochem. Biotechnol. 77, 91–103.
Lee, M., Rozeboom, H.J., de Waal, P.P., de Jong, R.M., Dudek, H.M., Janssen, D.B., 2017. Metal dependence of the xylose isomerase from piromyces sp. E2 explored by activity profiling and protein crystallography. Biochem. 56, 5991–6005.
Lira-Parada, P.A., Sinner, P., Kohlstedt, M., Kager, J., Wittmann, C., Herwig, C., Bar, N., 2022. Linking process and metabolic modelling for the estimation of carbon flux distribution in *Corynebacterium glutamicum* growth in spent sulfite liquor. IFAC-PapersOnLine 55, 228–233.
Lynd, L.R., Zyl, W.H.v., McBride, J.E., Laser, M., 2005. Consolidated bioprocessing of cellulosic biomass: an update. Curr. Opin. Biotechnol. 16, 577–583.
Mao, Y., Li, G., Chang, Z., Tao, R., Cui, Z., Wang, Z., Tang, Y.J., Chen, T., Zhao, X., 2018. Metabolic engineering of *Corynebacterium glutamicum* for efficient production of succinate from lignocellulosic hydrolysate. Biotechnol. Biofuels 11, 95.
Meiswinkel, T.M., Gopinath, V., Lindner, S.N., Nampoothiri, K.M., Wendisch, V.F., 2013. Accelerated pentose utilization by *Corynebacterium glutamicum* for accelerated production of lysine, glutamate, ornithine and putrescine. Microb. Biotechnol. 6, 131–140.
Moreno, M.S., Schneider, B.L., Maile, R.R., Weyler, W., Saier Jr, M.H., 2001. Catabolite repression mediated by the CcpA protein in *Bacillus subtilis*: novel modes of regulation revealed by whole-genome analyses. Mol. Microbiol. 39, 1366–1381.
Mutz, M., Brüning, V., Brüsseler, C., Müller, M.F., Noack, S., Marienhagen, J., 2024. Metabolic engineering of *Corynebacterium glutamicum* for the production of anthranilate from glucose and xylose. Microb. Biotechnol. 17, e14388.
Palmqvist, E., Hahn-Hägerdal, B., 2000. Fermentation of lignocellulosic hydrolysates. II: inhibitors and mechanisms of inhibition. Bioresour. Technol. 74, 25–33.
Pauli, S., Kohlstedt, M., Lamber, J., Weiland, F., Becker, J., Wittmann, C., 2023. Systems metabolic engineering upgrades *Corynebacterium glutamicum* for selective high-level production of the chiral drug precursor and cell-protective extremolyte L-pipecolic acid. Metab. Eng. 77, 100–117.
Qi, X.H., Yan, L.L., Shen, F., Qiu, M., 2019. Mechanochemical-assisted hydrolysis of pretreated rice straw into glucose and xylose in water by weakly acidic solid catalyst. Bioresour. Technol. 273, 687–691.
Rauzi, J., Tschirner, U., 2022. Enzymatic glucose and xylose production from paper mill rejects. Recycling 7, 24.
Rohles, C., Pauli, S., Giesselmann, G., Kohlstedt, M., Becker, J., Wittmann, C., 2022. Systems metabolic engineering of *Corynebacterium glutamicum* eliminates all by-products for selective and high-yield production of the platform chemical 5-aminovalerate. Metab. Eng. 73, 168–181.
Rohles, C.M., Giesselmann, G., Kohlstedt, M., Wittmann, C., Becker, J., 2016. Systems metabolic engineering of *Corynebacterium glutamicum* for the production of the carbon-5 platform chemicals 5-aminovalerate and glutarate. Microb. Cell Fact. 15, 154.
Rohles, C.M., Gläser, L., Kohlstedt, M., Giesselmann, G., Pearson, S., del Campo, A., Becker, J., Wittmann, C., 2018. A bio-based route to the carbon-5 chemical glutaric acid and to bionylon-6,5 using metabolically engineered *Corynebacterium glutamicum*. Green Chem. 20, 4662–4674.
Rumbold, K., van Buijsen, H.J.J., Overkamp, K.M., van Groenestijn, J.W., Punt, P.J., Werf, M.J.v. d., 2009. Microbial production host selection for converting second-generation feedstocks into bioproducts. Microb. Cell Fact. 8, 64.
Saha, B.C., 2003. Hemicellulose bioconversion. J. Ind. Microbiol. Biotechnol. 30, 279–291.
Saha, B.C., Qureshi, N., Kennedy, G.J., Cotta, M.A., 2015. Enhancement of xylose utilization from corn stover by a recombinant *Escherichia coli* strain for ethanol production. Bioresour. Technol. 190, 182–188.
Sasaki, M., Jojima, T., Inui, M., Yukawa, H., 2008. Simultaneous utilization of D-cellobiose, D-glucose, and D-xylose by recombinant *Corynebacterium glutamicum* under oxygen-deprived conditions. Appl. Microbiol. Biotechnol. 81, 691–699.
Sasikumar, K., Hannibal, S., Wendisch, V.F., Nampoothiri, K.M., 2021. Production of biopolyamide precursors 5-amino valeric acid and putrescine from rice straw hydrolysate by engineered *Corynebacterium glutamicum*. Front. Bioeng. Biotechnol. 9, 2021.
Schwechheimer, S.K., Becker, J., Peyriga, L., Portais, J.C., Sauer, D., Müller, R., Hoff, B., Haefner, S., Schröder, H., Zelder, O., Wittmann, C., 2018. Improved riboflavin production with *Ashbya gossypii* from vegetable oil based on ^{13}C metabolic network analysis with combined labeling analysis by GC/MS, LC/MS, 1D, and 2D NMR. Metab. Eng. 47, 357–373.
Stanton, R.C., 2012. Glucose-6-phosphate dehydrogenase, NADPH, and cell survival. IUBMB Life 64, 362–369.
Sun, X., Mao, Y.F., Luo, J.H., Liu, P., Jiang, M.R., He, G.M., Zhang, Z.D., Cao, Q.C., Shen, J., Ma, H.W., Chen, T., Wang, Z.W., 2022. Global cellular metabolic rewiring adapts *Corynebacterium glutamicum* to efficient nonnatural xylose utilization. Appl. Environ. Microbiol. 88.
Van Dyk, J.S., Pletschke, B.I., 2012. A review of lignocellulose bioconversion using enzymatic hydrolysis and synergistic cooperation between enzymes–factors affecting enzymes, conversion and synergy. Biotechnol. Adv. 30, 1458–1480.
van Winden, W.A., Wittmann, C., Heinzle, E., Heijnen, J.J., 2002. Correcting mass isotopomer distributions for naturally occurring isotopes. Biotechnol. Bioeng. 80, 477–479.
Voronovsky, A.Y., Ryabova, O.B., Verba, O.V., Ishchuk, O.P., Dmytruk, K.V., Sibirny, A. A., 2005. Expression of *xylA* genes encoding xylose isomerases from *Escherichia coli* and *Streptomyces coelicolor* in the methylotrophic yeast *Hansenula polymorpha*. FEMS Yeast Res. 5, 1055–1062.
Wang, Z.Q., Dien, B.S., Rausch, K.D., Tumbleson, M.E., Singh, V., 2019. Improving ethanol yields with deacetylated and two-stage pretreated corn stover and sugarcane bagasse by blending commercial xylose-fermenting and wild type *saccharomyces* yeast. Bioresour. Technol. 282, 103–109.
Weiland, F., Seo, K., Janz, F., Grad, M., Geldmacher, L., Kohlstedt, M., Becker, J., Wittmann, C., 2025. Metabolic engineering of *Corynebacterium glutamicum* for increased cis, cis-muconate production from plant-derived p-hydroxycinnamates via deregulated pathway flux and increased CoA intermediate availability. Metab. Eng. 92, 262–283.
Werner, F., Schwardmann, L.S., Siebert, D., Rückert-Reed, C., Kalinowski, J., Wirth, M.-T., Hofer, K., Takors, R., Wendisch, V.F., Blombach, B., 2023. Metabolic engineering of *Corynebacterium glutamicum* for fatty alcohol production from glucose and wheat straw hydrolysate. Biotechnol. Biofuels Bioproduct. 16, 116.
Wittmann, C., Heinzle, E., 2001. Modeling and experimental design for metabolic flux analysis of lysine-producing corynebacteria by mass spectrometry. Metab. Eng. 3, 173–191.
Wittmann, C., Heinzle, E., 2002. Genealogy profiling through strain improvement by using metabolic network analysis: metabolic flux genealogy of several generations of lysine-producing corynebacteria. Appl. Environ. Microbiol. 68, 5843–5859.
Wittmann, C., Kiefer, P., Zelder, O., 2004. Metabolic fluxes in *Corynebacterium glutamicum* during lysine production with sucrose as carbon source. Appl. Environ. Microbiol. 70, 7277–7287.
Wittmann, C., Kim, H.M., John, G., Heinzle, E., 2003. Characterization and application of an optical sensor for quantification of dissolved O_2 in shake-flasks. Biotechnol. Lett. 25, 377–380.
Wu, J.W., Dong, L.L., Liu, B.F., Xing, D.F., Zhou, C.S., Wang, Q., Wu, X.K., Feng, L.P., Cao, G.L., 2020. A novel integrated process to convert cellulose and hemicellulose in rice straw to biobutanol. Environ. Res. 186.
Xiao, H., Gu, Y., Ning, Y.Y., Yang, Y.L., Mitchell, W.J., Jiang, W.H., Yang, S., 2011. Confirmation and elimination of xylose metabolism bottlenecks in glucose phosphoenolpyruvate-dependent phosphotransferase system-deficient for simultaneous utilization of glucose, xylose, and arabinose. Appl. Environ. Microbiol. 77, 7886–7895.
Yang, T.H., Heinzle, E., Wittmann, C., 2005. Theoretical aspects of ^{13}C metabolic flux analysis with sole quantification of carbon dioxide labeling. Comput. Biol. Chem. 29, 121–133.

Yim, S.S., Choi, J.W., Lee, S.H., Jeon, E.J., Chung, W.J., Jeong, K.J., 2017. Engineering of *Corynebacterium glutamicum* for consolidated conversion of hemicellulosic biomass into xylonic acid. Biotechnol. J. 12.
Yim, S.S., Choi, J.W., Lee, S.H., Jeong, K.J., 2016. Modular optimization of a hemicellulose-utilizing pathway in *Corynebacterium glutamicum* for consolidated bioprocessing of hemicellulosic biomass. ACS Synth. Biol. 5, 334–343.
Zhu, S.D., Huang, W.X., Huang, W.J., Wang, K., Chen, Q.M., Wu, Y.X., 2015. Coproduction of xylose, lignosulfonate and ethanol from wheat straw. Bioresour. Technol. 185, 234–239.